January 2017

# Validating Precipitation Phase Measurements From Dual-Frequency Precipitation Radar On GPM Core Observatory Satellite

Benjamin Lott

Follow this and additional works at: https://commons.und.edu/theses

VALIDATING PRECIPITATION PHASE MEASUREMENTS FROM DUAL-FREQUENCY PRECIPITATION RADAR ON GPM CORE OBSERVATORY SATELLITE

by

Benjamin Thomas Lott
Associate of Science, Highland Community College, 2012
Bachelor of Science, University of North Dakota, 2015
Master of Science, University of North Dakota, 2017

A Thesis

Submitted to the Graduate Faculty

of the

University of North Dakota

in partial fulfillment of the requirements
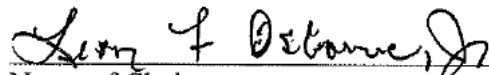
for the degree of

Master of Science

Grand Forks, North Dakota

August
2017
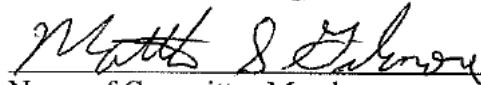
This thesis, submitted by Benjamin Lott in partial fulfillment of the requirements for the Degree of Master of Science from the University of North Dakota, has been read by the Faculty Advisory Committee under whom the work has been done and is hereby approved.

_____
Name of Chairperson

_____
Name of Committee Member

_____
Name of Committee Member

_____
Name of Committee Member

_____
Name of Committee Member

This thesis is being submitted by the appointed advisory committee as having met all of the requirements of the School of Graduate Studies at the University of North Dakota and is hereby approved.

_____
Grant McGimpsey
Dean of the School of Graduate Studies

_____
July 28, 2017
Date

<div align="center">PERMISSION</div>

Title        Validating Precipitation Phase Measurements from Dual-Frequency
Precipitation Radar On GPM Core Observatory Satellite

Department    Atmospheric Sciences

Degree       Master of Science

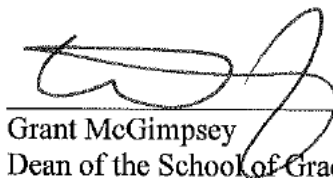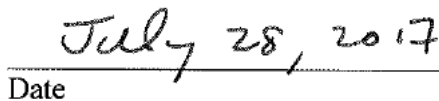    In presenting this thesis in partial fulfillment of the requirements for a graduate degree from the University of North Dakota, I agree that the library of this University shall make it freely available for inspection. I further agree that permission for extensive copying for scholarly purposes may be granted by the professor who supervised my thesis work or, in his absence, by the Chairperson of the department or the dean of the School of Graduate Studies. It is understood that any copying or publication or other use of this thesis or part thereof for financial gain shall not be allowed without my written permission. It is also understood that due recognition shall be given to me and to the University of North Dakota in any scholarly use which may be made of any material in my thesis.

<div align="right">Benjamin Lott<br>07/27/2017</div>

TABLE OF CONTENTS

LIST OF FIGURES

LIST OF TABLES

ACKNOWLEDGEMENTS

ABSTRACT

The purpose of this project is to validate precipitation measurements from the Global Precipitation Measurement (GPM)[1] Core Observatory (GPM-CO) satellite. The GPM-CO satellite is being used to detect falling rain and snow. Being able to detect rain builds off the success of the Tropical Rainfall Measuring Mission (TRMM), which provided reasonable rainfall estimates when compared to ground-based radars. Detecting falling snow was a key GPM-CO requirement that was to be met within three years the satellite's launch date of 27 February 2014. In this project, ground observations from Automated Surface Observing System (ASOS) and Automated Weather Observing Station (AWOS) was used to determine how well GPM-CO's Dual-frequency Precipitation Radar (DPR) can detect and classify precipitation phase. If GPM can detect precipitation, especially snow, it could lead to increased knowledge of fresh water resources. GPM can lead to a better understanding of the full picture of the water cycle and the effects precipitation has on the availability of fresh water. This can result in identifying patterns of precipitation systems over land. Results show that DPR struggles to detect solid precipitation (snow), but if detected, then DPR successfully determines the phase. DPR detects liquid precipitation better than solid precipitation but does not do as well at classifying it. Results also show that performance is not as good over complex terrain. These are promising results as they show that GPM-CO

---

[1] All acronyms can also be found in the Appendix

satellite meets its requirement of detecting falling snow. Other results show that it is successful at detecting and classifying rainfall as well.

CHAPTER I

INTRODUCTION/BACKGROUND

*a)  GPM Mission*

The Global Precipitation Measurement (GPM) mission, launched in 2014, is a joint mission led by the National Aeronautics and Space Administration (NASA) and the Japan Aerospace Exploratory Agency (JAXA) and consists of a constellation of precipitation measuring satellites from various countries (Hou et al. 2014; NASA 2017a). NASA has a Memorandum of Understanding with JAXA and the European Organisation for the Exploitation of Meteorological Satellites. For the participation of the Megha-Tropiques satellite, there are Memorandum of Understandings with Centre National D'Etudies Spatiales (CNES) of France and the Indian Space Research Organisation (ISRO).  Each of the satellites provides microwave sensor data to the mission while accomplishing their own operational goals and objectives. The GPM Core Observatory (GPM-CO) satellite serves as reference for the other members. Combined data from the constellation is available in near-real time.

The temporal sampling and spatial coverage depends on the number of partners that are in orbit. By the end of 2017, there will be seven satellites that will either be in commission or expected to still be in commission as seen in Figure 2 and summarized in Table 1. This thesis, herein, addresses the first of GPM's mission objectives, which include:

- Advancing precipitation measurements from space

1

- Improving knowledge of precipitation systems, water cycle variability, and freshwater availability

- Improving hydrological modeling and prediction

- Improving climate modeling and prediction

- Improving weather forecasting and 4D climate reanalysis
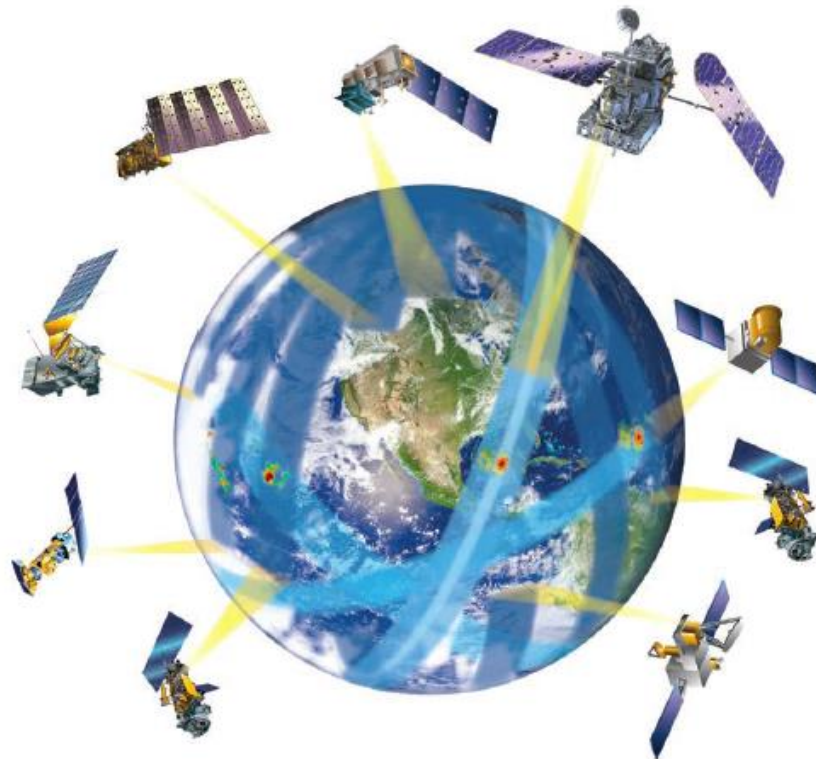


Figure 1. Global Precipitation Measurement (GPM) Constellation. GPM constellation of satellites that contribute microwave sensor measurements to the mission. Satellites shown include US-Japan GPM-CO (upper right corner), Indo-French Megha-Tropiques, GCOM-WI of Japan, European MetOp satellites, and United States satellites: DMSP, POES, suomi-NPP, and JPSS (acronyms found in Appendix A) (Figure 1 from Hou et al 2014).
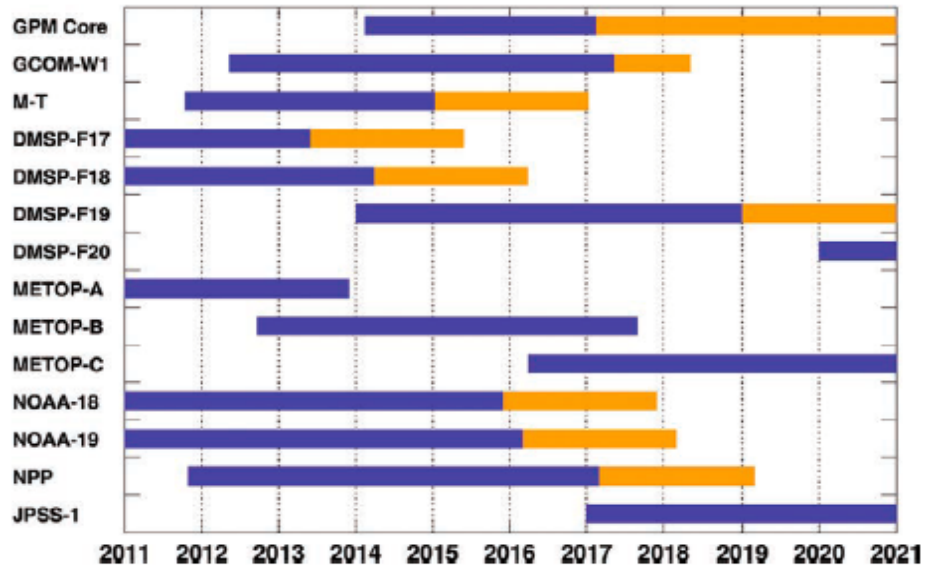
Figure 2. Launch Schedules. Estimated launch schedules and life spans of satellites in the GPM constellation. Blue denotes the main mission phase, while yellow denotes an extended mission phase. (Figure 3 from Hou et al. 2014)

Table 1: Satellites Mentioned in Figure 2 Definitions, origins, and start dates, for satellites that were mentioned in Figure 2. Except where indicated, all operations are ongoing as of July 2017. (Gruss 2016; NASA 2012; NASA 2017c; NOAA 2017a; Rémy et al. 2015).
* The M-T satellite is still in operation, but the microwave imager on board stopped working on January 26, 2013.
**Operation ended.

| Satellite Acronym | Acronym Definition | Origin | Operation Start Date |
|---|---|---|---|
| GPM | Global Precipitation Measurement | USA & Japan | 27 February 2014 |
| GCOM-W1 | Global Change Observation Mission-Water 1 | Japan | 17 May 2012 |
| M-T | Megha-Tropiques | India & France | October 2011* |
| DMSP (F17-20) | Defense Meteorological Satellite Program | USA | F17: 4 November 2006 F18: 18 October 2009 F19: 3 April 2014** F20: cancelled (not launched) |
| MetOp (A-C) | | Europe | A: 19 October 2006 B: 17 September 2012 C: Expected 2018 |
| NOAA (18-19) | National Oceanic and Atmospheric Administration | USA | 18: 20 May 2005 19: 6 February 2009 |

3

| | | | |
|---|---|---|---|
| Table 1 Continued | | | |
| NPP | National Polar-Orbiting Operational Environmental Satellite System (NPOESS) Preparatory Project | USA | 28 October 2011 |
| JPSS-1 | Joint Polar Satellite System | USA | Expected 2018 |

GPM provides the next generation of precipitation products by improving on the current generation of products that are centered around the Tropical Rainfall Measuring Mission (TRMM). GPM is expected to improve the accuracy of precipitation estimates including light rain and cold-season solid precipitation, which were lacking from TRMM. Microwave radiometers throughout the constellation provide unified precipitation estimates (Hou et al. 2014).

*b) GPM Satellite and DPR*

The GPM-CO satellite was developed by NASA and JAXA to build on the success of the Tropical Rainfall Measuring Mission (TRMM) satellite and was launched 27 February 2014. The TRMM satellite was launched in November 1997, but went out of commission on 15 April 2015 (Pierce 2017). Much like GPM's goal, the main goal of TRMM was to advance the knowledge of the global water and energy cycles. It had a low inclination orbit of 35° and originally orbited at an altitude of 350 km. The altitude was later increased to 402.5 km to reduce drag and expand fuel life. The phased array precipitation radar (PR) on TRMM was the first and only spaceborne radar until the launch of the GPM. The PR had two goals: produce 3-D structures of rainfall and obtain high quality rainfall measurements (Alder et al. 2007). TRMM rain rate measurements agreed with Melbourne, Florida ground validation

radar. For 24 overpass cases, the average correlation coefficient was 0.89 (Hou 2000; Liao and Meneghini 2001). Liao and Meneghini (2009) expanded their study to 210 overpasses during a 10-year period and found that rain rates from TRMM still agreed with the Melbourne site, despite underestimates of convective rain. Due to variabilities in climate, surface background, and raindrop size distribution PR's performance can be affected, so other geographical areas should be studied (Liao and Meneghini 2009). TRMM was so successful, that it set the standard for spaceborne precipitation measurements and was often called the "flying rain gauge" (Alder et al. 2007). TRMM has been used in many applications from studying the climate to improving precipitation measurements. The data has been used in operational settings to help monitor tropical storms and rainfall. It has also been incorporated into numerical weather prediction (Braun 2011). Due to the success of TRMM, the GPM mission was formed and the planning for the GPM-CO satellite began just a few years after the launch of TRMM (Hou 2000).

GPM-CO flies a non-sun-synchronous orbit with inclination of 65° and an altitude of 407 km +/- 10 km (Hou et al. 2014; Skofronick-Jackson et al. 2016; NASA 2017d). A non-sun-synchronous orbit was chosen, because it allows for sampling diurnal variabilities during seasons and provides broad latitudinal coverage. Figure 3 shows an example of the path of a GPM-CO overpass. The design life of GPM-CO is three years, but has fuel that will last a minimum of five years (Hou et al. 2014). If the instruments do not fail, then GPM-CO could last twenty or more years (Skofronick-Jackson et al. 2016b). Multiple maneuvers can be made depending on the needs of the satellite. Inclination Adjust Maneuvers are performed to alter the orbit of GPM-CO. Drag Makeup Maneuvers are used to counteract atmospheric drag

and occur every one to three weeks depending on the drag effects. Risk Mitigation Maneuvers are performed only to avoid space debris (NASA 2017d).
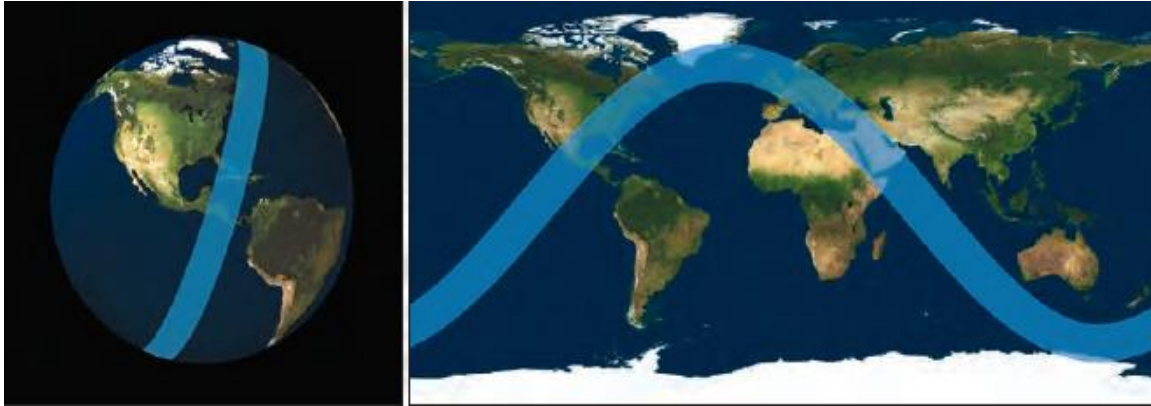


Figure 3. GPM Orbit Path. The orbital path and footprint of the GPM satellite as viewed on a globe (left) and cylindrical map projection (right).

The GPM-CO satellite is the first satellite equipped with a dual-frequency phased array precipitation radar (DPR), which was developed by JAXA and the National Institute of Information and Communications Technology of Japan (NICT). It can distinguish between solid, mixed, and liquid phase precipitation (Hou et al. 2014). A phased array radar is made up of a stationary, flat panel. To move a phased array radar, the beams are electronically steered, but this shift is maximized to 60° to the left and right (Wolff 2017; NSSL 2017). The DPR consists of two radars: Ka-band precipitation radar (KaPR) and Ku-band precipitation radar (KuPR), which operate at 35.5 GHz and 13.6 GHz, respectively. The KuPR was modeled after the TRMM PR. The KaPR has a scan width of 120 km while the scan width of the KuPR is 245 km (also see Fig. 7). The two radars have a vertical range resolution of 250 km and a minimum detectable signal (MDS) greater than 18 dBZ. KaPR has a high-sensitivity mode that has a vertical range resolution of 500 m and a MDS of 12

dBZ. This mode is used to sample when the Ka-band and Ku-bands are interlaced, meaning that the two bands are just offset from each other instead of matching footprint for footprint (Hou et al. 2014). KaPR is used to improve sensitivity and can detect light rain and snow, and KuPR can detect heavy rain. Together, they can detect rain and snow from the tropics to high-latitude areas (JAXA 2017a). Having two frequencies allows GPM to provide quantitative measurements on the particle size distribution as well as gain information on physical processes of precipitation (Hou et al. 2014). The two bands also have three scan modes: High Sensitivity Scan (HS), Matched Scan (MS), and Normal Scan (NS). Figure 4 is a diagram showing these different scans. The Normal Scan is the KuPR. The Matched Scan is when the KaPR and KuPR beam positions match whereas the High Sensitivity Scan (HS) is when the KaPR and KuPR positions are overlapped but offset from each other (JAXA 2017a).
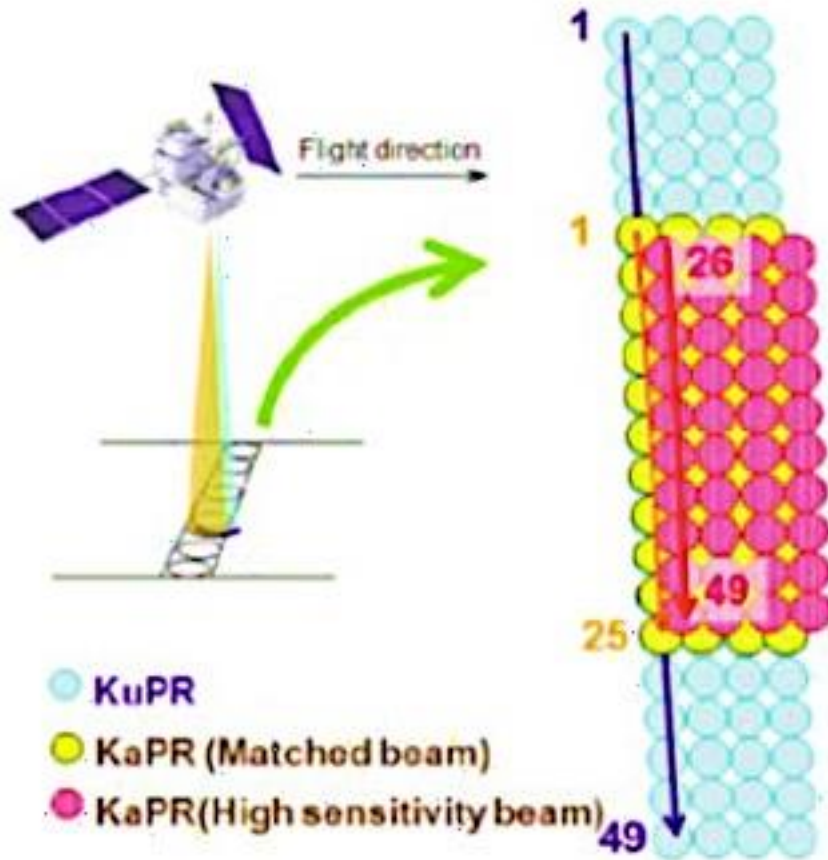
Figure 4. DPR Footprint. With the radar moving left to right, the footprint is shown for HS, MS, and NS. HS is represented by the red, MS by yellow, and NS by blue. The numbers indicate the angle bins of footprints (Figure 1.3-2 from JAXA 2017a).

Figure 5 provides an early visual of the capabilities of these two bands when measuring tropical rainfall and snowfall/rainfall in the mid to high latitudes. This figure shows that the Ku band radar frequency is best for measuring all but the heaviest tropical precipitation while the Ka band is better for measuring all but the lightest mid-to-high latitude precipitation. For the range of precipitation rates where both bands can measure well, moderate precipitation rates will be covered as well as the majority of heavier rain and snow in the mid-to-high latitudes and majority of lighter rain in the tropics. The GPM-CO satellite was designed to detect rainfall rates as low as 0.2 mm h$^{-1}$. Studies have shown that it has the capability of

detecting liquid-equivalent snowfall rates above 0.5 mm h^{-1} (Skofronick-Jackson et al. 2015).
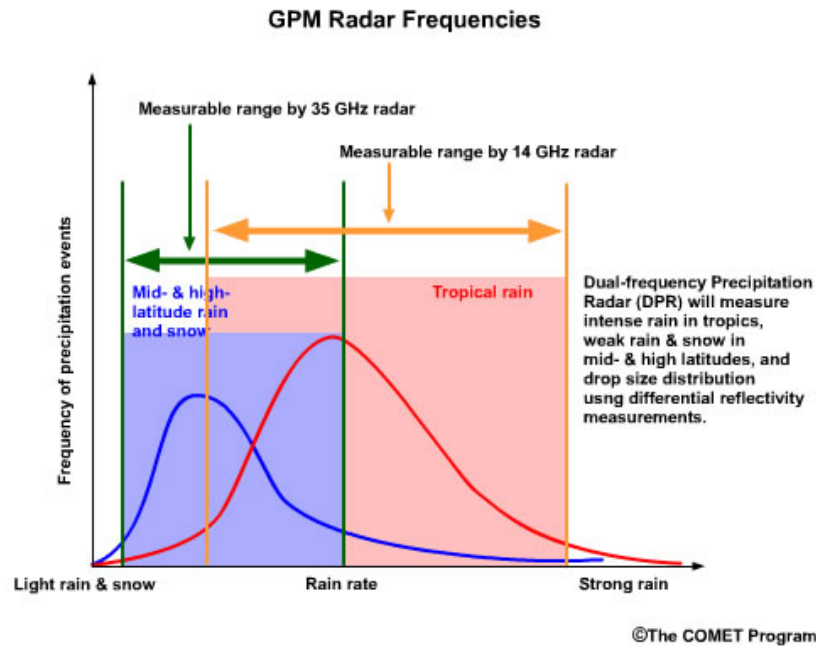


Figure 5.  GPM Radar Frequencies. The frequency of precipitation events in the tropics (red) compared to the mid-to-high latitudes (blue) as a function of precipitation rate.  The measurable ranges of the KuPR and KaPR radar bands are shown with blue and red shading, respectively (UCAR 2006).

*c)  Ground Validation and Past Work*

Early ground validation efforts for the GPM mission and pre-launch of the GPM-CO satellite involved using ground radars. A validation network of radars consisting of WSR-88D, the Gosan (RSGN) S-band radar is located near the tip of Jeju Island and provided by the Korea Meteorological Administration (KMA), and Advanced Radar for Meteorological and Operational Research at University of Huntsville (Alabama), Darwin C-band dual-polarization radar operated by Australian Bureau of Meteorology, and Kwajalein (KWAJ) radar on the Marshall Islands made up the collection. These radars were used in algorithm development and would be used to study GPM-CO measurements (Schwaller and Morris

9

2011). Field campaigns helped contribute to the validation needs of the GPM mission as well. Completed campaigns pre-launch of GPM-CO included the Canadian CloudSAT/Calipso Validation Program (C3VP), Light Precipitation Evaluation Experiment (LPVEx) Mid-Continent Convective Clouds Experiment (MC3E), GPM Cold-season Precipitation Experiment (GCPEx), and Iowa Flood Studies (IFloodS). The GPM team took part in C3VP, which the University of Massachusetts provided a ground-based 3-frequency (W, Ka, and Ku) Advanced Multi-Frequency Radar that was used in measuring some of the snow events. LPVEx in 2010 was conducted to understand the ability of CloudSat and GPM to detect light precipitation. (NASA 2017b).

Some of these experiments also used airborne-based radars. MC3E was the first physical ground validation effort of GPM. Part of this project included measurements with a high-altitude airborne Ka/Ku band radar. These measurements were compared with ground-based polarmetric radars to help refine the basis of DPR retrievals. GCPEx provided airborne and ground-based measurement data for snowfall algorithm developers. During IFloodS, multifrequency polarmetric radars, rain gauges, and disdrometers provided measurements that were coupled with land surface and hydrological models. Comparing the measurements with the models helped understand the uncertainties in satellite precipitation measurements and how that impacts flood forecasting (Hou et al. 2014).

The Integrated Precipitation and Hydrology Experiment (IPHEx) was a post-launch ground validation campaign that took place in 2014 and 2015. IPHEx was performed over the Southern Appalachians. One goal of IPHEx was to use ground and airborne measurements to help improve satellite precipitation measurements over terrain (Barros et al.

2014). The Olympic Mountains Experiment (OLYMPEX) occurred during the 2015-2016 winter season. OLYMPEX was another field campaign to help improve the GPM-CO satellite's precipitation measurements. This experiment also used numerous ground and air measurements. NASA's own aircraft (DC-8 and ER-2) were used to mimic the satellite as an overpass of the satellite over any given location occurs only twice a day. The University of North Dakota Citation flew with a probe to measure ice particle sizes and concentrations, which this information can be used in GPM's algorithms to convert measurements to precipitation rates. The data from this campaign will fulfill the need to improve retrieval algorithms over mountainous terrain (Houze et al. In press).

In addition to field campaigns, other studies have investigated DPR measurements using a variety of validation methods. DPR agreed reasonable well with simulations from the Nonhydrostatic Icosahedral Atmospheric Model (NICAM) of precipitation patterns and bright band heights in frontal precipitation. NICAM simulated higher echo tops than DPR, suggesting there is a bias in NICAM of mixing ratios of snow and graupel. The agreement between the simulations and DPR provides the possibility of using GPM precipitation data in numerical weather prediction (Kotsuki et al. 2014). Hamada and Takayabu (2016) showed that GPM's DPR detects precipitation better than the TRMM PR because DPR is effective in detecting light precipitation over convection-suppressed areas and in lower levels of anvil clouds. In another study (Le et al. 2016), GPM's dual-frequency method (discussed in Section 2) agreed well with the TRMM legacy Ku-only algorithm. It was also determined that melting layer detection agrees well with NASA's S-band dual-polarized (NPOL) and NEXRAD radars. In this same study, Le et al. 2016 introduced a new algorithm, Snow Index,

to differentiate between snow and no snow. Snow Index is an experimental product and undergoing testing, but comparisons with ground radars indicate promising results (Le et al. 2016; Chandrasekar et al. 2016). GPM data has been used in the NASA Land Information System (LIS). LIS uses observations from satellites like GPM and the Soil Moisture Active Passive (SMAP) satellite to provide analyses and short-term forecasts of soil moisture (Skofronick-Jackson et al. 2016a).

A recent study, Speirs et al. 2017, compared DPR with MeteoSwiss ground-based radars in the Swiss Alps and Plateau. Speirs et al. found that DPR products are more reliable during the summer and over flatter terrain. Comparing precipitation rates and using a threshold of at least 0.15 mm/hr, dual-frequency products have a small bias of -14% but since MeteoSwiss radars also exhibit a small bias, DPR may be closer to unbiased. They found that DPR misses 24% of all precipitation events, and this is likely higher as the MeteoSwiss radars also miss events. During the winter, DPR measured 49% of the total rainfall accumulation in complex terrain. In general, DPR was found to underestimate rainfall rates.

This study also applied detection metrics to help measure the performance of DPR. These metrics include the probability of detection (POD), false alarm rate (FAR), and Heidke Skill Score (HSS). POD is calculated using

$$POD = \frac{TP}{TP + FN} \quad (1.)$$

where *TP* is the total number of true positives and *FN* the total number of false negatives. True positive indicates when the test and reference both detect precipitation. False positive (FP) is when precipitation is detected by the test but not by the reference. FAR is calculated using

$$FAR = \frac{FP}{TP + FP} \quad (2.)$$

The Heidke Skill Score (HSS) or Cohen's Kappa is calculated using

$$HSS = \frac{2[TP(TN) - FP(FN)]}{(TP + FN)(FN + TN) + (TP + FP)(FP + TN)} \quad (3.)$$

where true negative, *TN,* represents the incidents of when both test and reference do not detect precipitation. HSS is a test comparing the performance of what is being tested to random guessing. An HSS of one means the measurement is perfect, and zero means the measurement is as good as random guessing. If HSS happens to be negative, then the measurement is worse than random guessing. Their results are shown in Table 2 for complex and flat terrain and were calculated for occurrences when MeteoSwiss Radars and DPR scanned above and below the melting level.
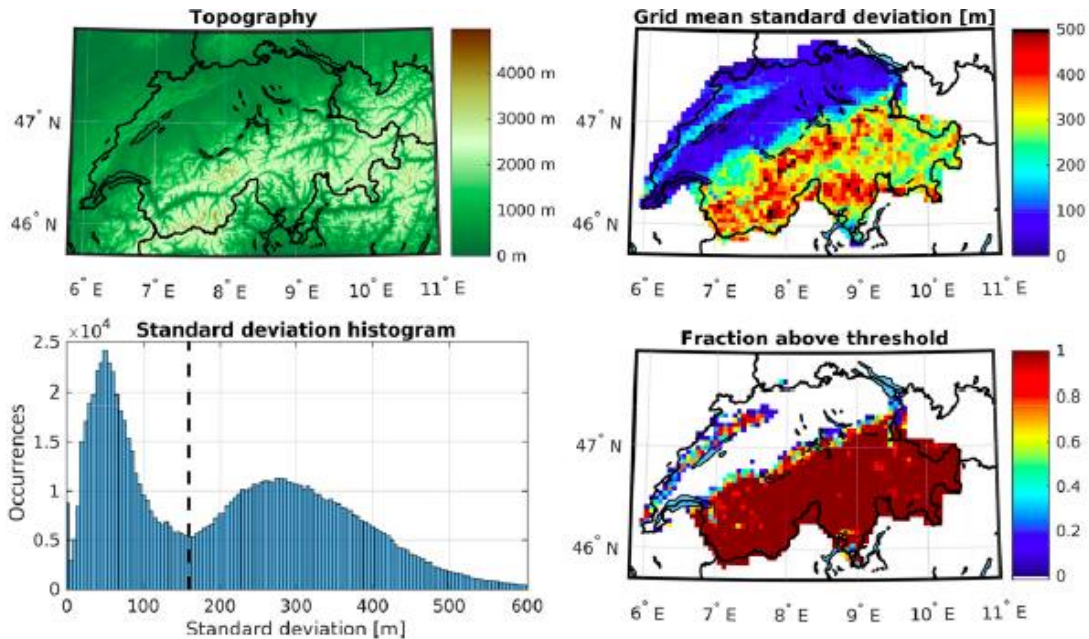


Figure 6. Switzerland Topography. (Top Left) The Shuttle Radar Topography Mission DEM of Switzerland and surrounding area. (Top Right) Mean of the standard deviation of the DEM of each measurement that lies within each 5-km grid square. (Bottom Left) Histogram of standard deviation of DEM for each footprint, and the black dashed line represents the

160-m threshold used to define flat and complex terrain. (Bottom Right) The fraction of footprints that fall within a 5-km grid box and exceed the 160-m terrain threshold (Figure 3 from Speirs et al. 2017).

Speirs et al. (2017) differentiate between complex and flat terrain, by calculating the standard deviation of the SwissTopo 25 m digital elevation model (DEM) using a 2.5 km radius from the center of a DPR pixel as a discriminator. The threshold determined for complex and flat terrain was 160 m. Figure 6 (above) shows the terrain of Switzerland, the grid mean standard deviation, a histogram of the standard deviation, and areas exceeding the threshold. They defined above the melting layer as levels at or greater than 100 m above the 0°C level and below the melting layer was defined at levels at or greater than 800 m below the 0°C level.

Table 2. Speirs et al. Results. The detection metrics for complex and flat terrain when comparing DPR's Matched Scan with MeteoSwiss Radars. This was done for when MeteoSwiss Radars and DPR scanned above or below the melting layer (Adapted from portions of Tables 4 and 5 in Speirs et al. 2017).

| Radars and scans relative to melting layer | | Complex Terrain | | | Flat Terrain | | |
|---|---|---|---|---|---|---|---|
| MeteoSwiss Radar | DPR Matched Scan | POD | FAR | HSS | POD | FAR | HSS |
| Above | Above | 0.366 | 0.0394 | 0.505 | 0.685 | 0.0113 | 0.77 |
| Above | Below | 0.227 | 0.167 | 0.35 | 0.174 | 0.0625 | 0.791 |
| Below | Above | 0.649 | 0 | 0737 | 0.614 | 0 | 0.687 |
| Below | Below | 0.799 | 0.0568 | 0.843 | 0.783 | 0.0411 | 0.854 |

In addition to comparing satellite measurements with ground observations, other validation efforts involve inter-comparing satellite precipitation products and analyzing data to ensure that mission requirements are met. Analyzing the performance of each product

14

allows room for changes in algorithms for future versions of data. Some ground validation products used are those from the National Severe Storms Laboratory (NSSL)/University of Oklahoma Multi-Radar/Multi-Sensor (MRMS). MRMS incorporates data from all polarimetric WSR-88D radars (NEXRAD), automated rain gauge networks, and model analysis in CONUS and southern Canada. The gridded quantitative precipitation estimates (QPE) provide a reference to directly evaluate GPM precipitation products (Skofronick-Jackson et al. 2016a).

While prior studies have illustrated that GPM is an improvement of TRMM and that precipitation rates from DPR agree with ground-based radars, it is clear that more work needs to be done on validating DPR's precipitation phase measurements. Thus, the thesis work herein attempts to begin to fill that gap.

*d) Precipitation Measurements*

Precipitation measurements of rain and snow are taken mostly by instrumented ground stations equipped with gauges. There are several rain gauges that exist like weighing gauges, tipping-bucket gauges, and even simple cans. Some rain gauges are protected with wind guards to obtain more accurate measurements. Precipitation falls in the orifice and is collected by the rain gauge. From this collection, the precipitation amount is measured. While simple cans would require a manual reading, weighing gauges and tipping-bucket gauges have been automated to save on costs (Kidd et al. 2017). Surface weather stations are equipped with sensors to determine the precipitation phase. The phase of precipitation is determined by a Present Weather Identifier sensor. This sensor can identify snow and rain. A

separate sensor, Freezing Rain sensor, is used to identify freezing rain (NWS 2015). One manufacturer of Present Weather Identifier sensors, Campbell Scientific, designs their instruments to identify precipitation particles from their scattering properties and fall velocities. Air temperature is also used to determine the observation. Continuous, high-speed measurements help reduce error when identifying mixed precipitation (Campbell Scientific 2014).

There are large networks of precipitation gauges throughout the world. The World Meteorological Organization (WMO) Global Telecommunication System (GTS) provides global meteorological data from 8,000 to 12,000 rain gauges. The Global Precipitation Climatology Project (GPCP) at the Global Precipitation Climatology Centre (GPCC) has organized a comprehensive set of daily data. As of 2015, 180 institutions, including WMO, using about 100,000 gauge locations that have reported at least once since 1901 contribute to the GPCC database. However, to construct a climatological analysis, the GPCC established a ten-year minimum constraint to maintain continuous data from any station. Enforcing this restriction results in about 73,586 stations. Considering the area of just the rain gauges from these two databases and assuming an orifice size of 246 cm$^2$, the area these gauges cover is small. Assuming the maximum number of gauges from GTS, the total area represented is 295 m$^2$, just larger than the size of the center circle of a soccer field. GPCC gauges cover an area of 1,612 m$^2$, similar area of four basketball courts. If each one was representative of precipitation falling over an area with 5 km radius and no overlap of stations, this represents about 1% of Earth's surface. Figures 7 and 8 show the distance from any one point on Earth's surface to a GTS and GPCC gauges, respectively. From 60°N-S latitude (similar to GPM

16

Core Observatory satellite's scan range), 6.5% of land lies within 10 km of a gauge while

23.0% lies with 25 km (Kidd et al. 2017). Due to GPCC's high number of rain gauges, the

distance to a gauge from any one location decreases in many areas.
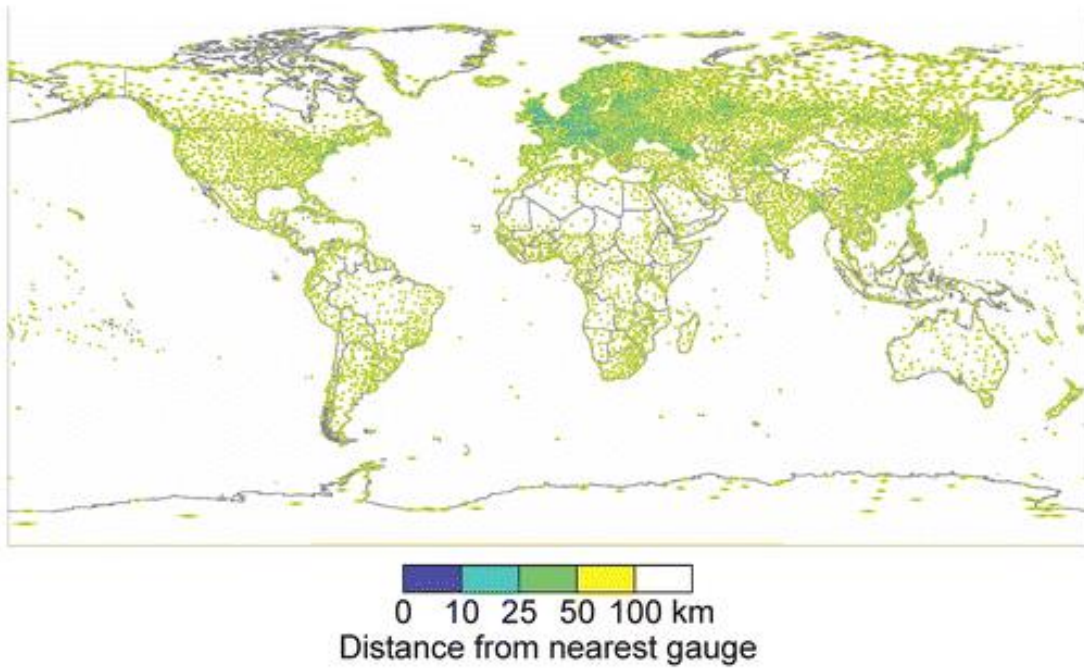


Figure 7. GTS Gauges. Map showing distance to nearest GTS gauge. Any distance beyond 100 km is blank (Figure 1 from Kidd et al. 2017).
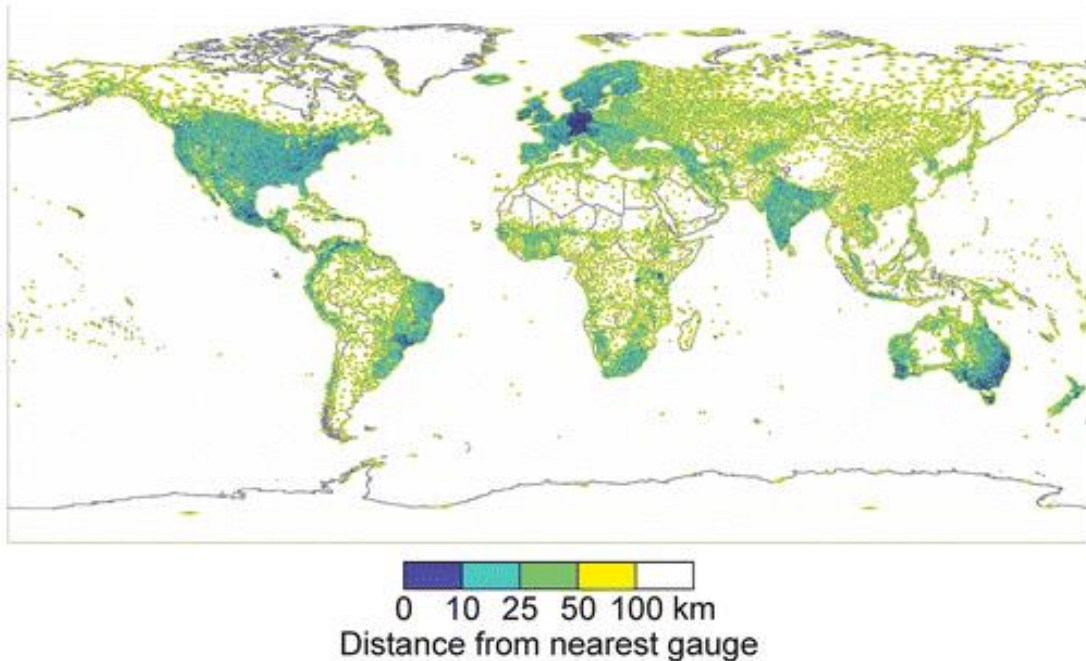
Figure 8. GPCC Gauges. Map showing distance to nearest GPCC gauge. Any distance beyond 100 km is blank (Figure 2 from Kidd et al. 2017).

To fill the gaps between gauges, ground-based radars can also be used to estimate precipitation amounts as well as the phase. The United States has 160 Next Generation Radar (NEXRAD) sites in all fifty states, Puerto Rico, Guam, and some military bases in Asia and the Azores. However, there are also gaps in radar coverage, possibly more than rain gauges. Earth's curvature is a weak point to weather radars. NEXRAD scans at a 0.5° angle, but the beam elevation increases as the distance away from the radar increases. This limits the radar's ability to scan close to the ground (Mersereau 2015). As the radar beam travels farther away from the radar, the more detail is lost about what the beam identifies due to less power. Due to Earth's curvature, the farther the beam travels, the higher it is above the ground. Density differences in the atmosphere can steer the beam, which then gives false beam heights while possibly missing precipitation. Other limitations that include attenuation and the Doppler Effect. Attenuation is when the radar beam hits something large, like a hail

18

core, and is then limited to how much it can scan beyond that point. The Doppler Effect is the radar's limitation to scan at far ranges and high velocities (SKOW 2013). Gaps in radar coverage are common in mountainous areas, but also in populated areas. For example, there is a gap in central North Carolina near Charlotte and Greensboro. These gaps can be seen in Figure 9, which shows NEXRAD coverage in the United States If a radar stops working, then the area covered by that radar is lost (Mersereau 2015).

Differences between the NEXRAD radars and DPR are based on what they are designed to do. NEXRAD radars are designed to detect precipitation near the surface by measuring horizontally. DPR is designed to detect not only precipitation, but characteristics of droplets in clouds while measuring in the vertical direction. The NEXRAD radars can scan 360° in the horizontal and can increase the beam angle to scan higher in the atmosphere. They operate in the S-band and have a frequency around 3 GHz with MDS values below 0 dBZ (NOAA 2017b). With a lower frequency and MDS than DPR, they are designed to detect larger precipitation particles, as found in cloud bases. The higher frequencies on DPR allow it to see finer sized particles found near the top of clouds. These smaller drops will not be detected by NEXRAD radars due to its frequency and maximum scan height. NEXRAD and KuPR both experience Rayleigh scattering, but the KaPR will not experience Rayleigh scattering due to the higher frequency allowing DPR to measure drop size distributions (Iguchi et al. 2016). A satellite has a limited amount of space for instruments, so not only does that affect the type of radar used, but also the power used to run it. As mentioned earlier, DPR is a phased array radar, which has no moving parts (Hou et al. 2014). GPM is powered by solar panels whereas ground based radars have unlimited power sources.
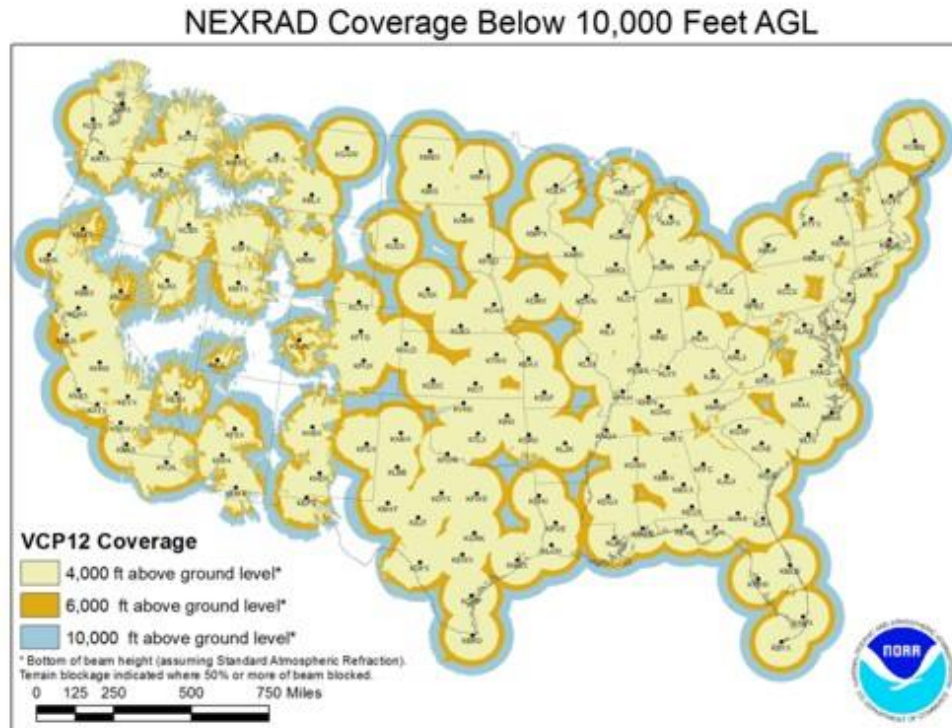
Figure 9. NEXRAD. Next-Generation Radar (NEXRAD) coverage below 10,000 feet above ground level (AGL) in the contiguous United States (Accessed from NOAA 2016)

To help fill these radar gaps, crowdsourcing programs have been developed. The Community Collaborative Rain, Hail, and Snow Network (CoCoRaHS) originated at Colorado State University and is a community that utilizes volunteers to make meteorological observations. The reports are collected, and the resulting data is used by many disciplines. Figure 10 illustrates the locations of CoCoRaHS active stations as of June 2017 (CCC 2016).
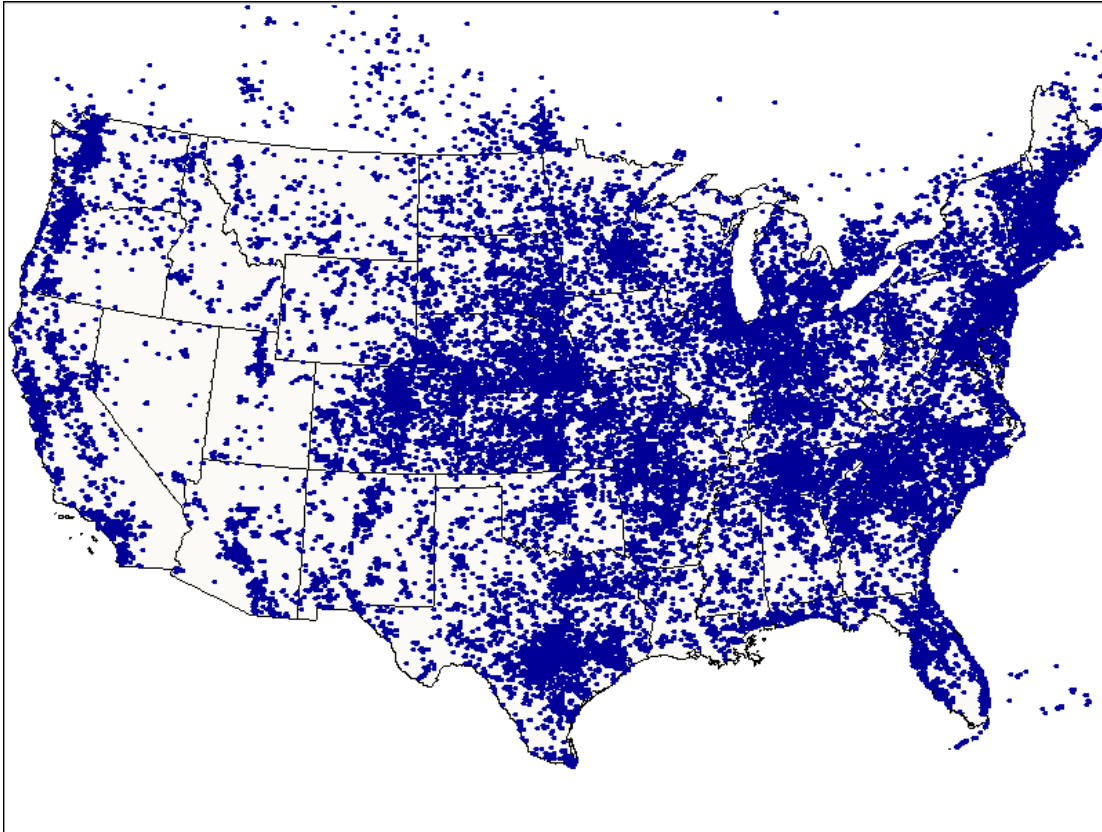
Figure 10. CoCoRaHS. CoCoRaHS active stations as of June 2017 (Accessed from CCC 2017).

Similarly, the UK Met Office developed Weather Observations Website (WOW) where users anywhere in the world can submit observations via mobile app or the website. They developed the WOW Schools program to encourage schools to submit weather observations. All observational data is shared with government and public agencies (Gilbert 2016). Other organizations, companies, and programs have crowdsourcing data including Weather Underground, NOAA's Citizen Weather Observer Program and Meteorological Phenomena Identification Near the Ground (mPING), Netatmo brand personal weather stations, and the UK Snow Map. Social media offers another source for weather observations from the public (Kidd et al. 2017). ASOS and AWOS ground observations give the weather right at the

surface and are constantly maintained. These serve as the best reference for studying measurements at the surface.

*e) Motivation*

Comparing Figures 9 and 10 reveals that there are still gaps in coverage, after accounting for CoCoRaHS and WSR88D. Some obvious gaps are northern Minnesota, eastern parts of Montana, and the Rocky Mountains. These gaps in coverage could possibly be filled by the GPM-CO satellite radar. Figure 11 illustrates that during an orbit, the Dual-frequency Precipitation Radar (DPR) has continuous coverage over land as well as water, however for the study herein, only the over-land data is used.



Figure. 11. Ground Radar Coverage with GPM Scan. Ground radar coverage in the contiguous United States. Overlap of radars is shaded in green, yellow, and red. An example orbit showing DPR coverage that would fill in gaps of ground radar coverage (Image from Hanson and Gray 2012).

Lott and Skofronick-Jackson (2017) studied DPR's performance of correctly classifying the phase of solid precipitation. They chose a DPR scan for 30 individual events, known to produce snow, to study that occurred from March 2014 through February 2016. These events occurred over land and east of the Rocky Mountains. Using ground observations as validation, and assuming that DPR detected any precipitation, for light snow observations, DPR correctly classified the precipitation as solid phase for over 99% of the time. For moderate snow observations, this number was 100%. It should be noted that DPR fails to detect any precipitation most of the time, such that the overall detection rates are poor.

This current study is an extension of the Lott and Skofronick-Jackson (2017) work, except by using *all* ground observations from the CONUS between March 15, 2014 and March 15, 2016 as validation. Unlike Lott and Skofronick-Jackson 2017, all areas of CONUS including the Rocky Mountains were studied herein. To test the performance of DPR, a skill score was computed and assigned to the DPR-determined phase of precipitation as compared to the ground observations ("ground truth").

The procedure of how the DPR determines the phase of precipitation is discussed in Section 2. More details on the methodology of this study are in Section 3. Results are presented in Section 4, Section 5 contains discussion and conclusions of the study, and Section 6 proposes possible future work.

CHAPTER II

GPM DUAL-FREQUENCY PRECIPITATION RADAR ALGORITHM

This section summarizes parts of the Dual-frequency Precipitation Radar (DPR) Level 2 (L2) algorithm. A flowchart of this algorithm is displayed in Figure 12. For the full process, please refer to Iguchi (2016). To begin the process of detecting precipitation, the radar sends out a signal and receives an echo from precipitation, if present. The Preparation (PREP) module identifies precipitation/non-precipitation pixels throughout the column. The Classification (CSF) module classifies each precipitation pixel as stratiform, convective, or other. The Raindrop Size Distribution (DSD) module determines the phase of precipitation.
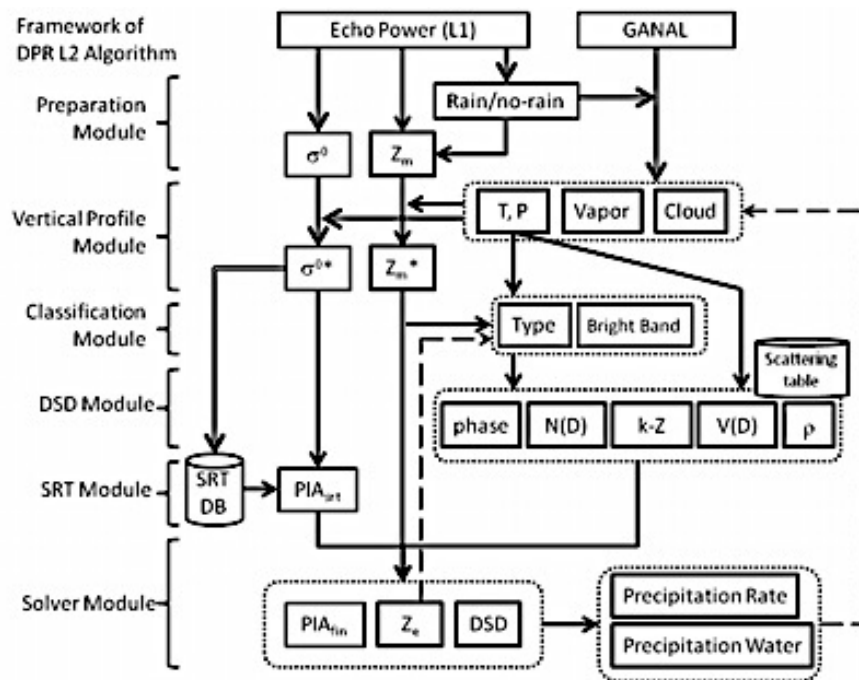


Figure 12. DPR L2 Algorithm Flowchart. Flowchart of the DPR L2 Algorithm (Figure 2 from Seto et al. 2011).

In PREP module, data that is missing is determined from the Ku-band Level-1B product that includes radar echo and other variables such as latitude/longitude and elevation. The *binClutterFreeBottom* is an estimate of the range bin number of the clutter-free bottom and is estimated using *echoPower*. Clutter here refers to unwanted echoes from ground clutter. The PREP module is executed for all range bins above *binClutterFreeBottom* except for missing data. If *echoSignalPower*, calculation shown below, meets a certain threshold, then rain is detected. This threshold may vary in each observation, but is based on the noise power. The signal/noise ratio must be greater than four in three consecutive/adjacent vertical bins.

$$Pecho = pow\left(10.0, \frac{(double)echoPower}{10}\right) \quad (4.)$$

$$Pnoise = pow\left(10.0, \frac{(double)noisePower}{10}\right) \quad (5.)$$

$$Psignal = Pecho - Pnoise \quad (6.)$$

$$echoSignalPower = 10 * log10(Psignal) \quad (7.)$$

In these equations, *echoPower* is the DPR-received power. If *Psignal* is negative, a missing value flag is stored in *echoSignalPower*. Results of the rain/no rain classification from the range bins are stored in *flagEcho,* which is used for the angle bins classification. The results from the angle bins are stored in *flagPrecip* which is used by other modules downstream.

The CSF module classifies precipitation as stratiform, convective, or other, based upon the existence and characteristics of a radar bright band in the vertical profile. (Type 'other' is the existence of only clouds or noise.) The dual frequency algorithm uses the measured dual frequency ratio ($DFR_m$) method and the single frequency result from the Ku-only module. The $DFR_m$ is a type of vertical profiling method with classifications of stratiform, convective,

and transition. Transition is stratiform transitioning to convective. However, this method is unified with the Ku-only module, so the rain types stay as stratiform, convective, and other.

The $DFR_m$ method uses the difference between the measured reflectivity of the Ku and Ka bands as shown in the equation below:

$$8. DFR_m = 10 \log_{10}\big(Z_m(K_u)\big) - 10 \log_{10}\big(Z_m(K_a)\big) \quad (8.)$$

where $Z_m$ is the measured linear reflectivity ($mm^6$ $m^{-3}$). $Z_m$ is the result of attenuation correction for non-precipitation particles and is provided below:

$$Z_m = Z_e(r)A_P(r) \quad (9.)$$

where $Z_e(r)$ is the effective radar reflectivity factor at range r and $A_P(r)$ is the attenuation by precipitation particles. Besides classifying precipitation type, $DFR_m$ is also used to detect the melting layer which can be compared with the radar bright band (BB) identified using the Ku-only method. The Ku method uses radar reflectivity, corrected for attenuation, to detect a BB. A sharp peak in radar reflectivity is usually observed in the non-slanted (purely vertical) beam profile when a BB is present. This is the so-called "vertical method" for detecting a BB. For the "horizontal method", a BB may be detected by screening nearby pixels and is effective for finding a BB in a slanted beam observation. Through either method, if a BB is detected, the boundaries of the BB may be determined. The bottom is the point where there is the largest change in slope of reflectivity ($Z$) just below the BB peak. This lower boundary, "B", is determined before the upper boundary, "A".

Point B, the lower boundary, is the location where $Z$ becomes smaller than $Z$ at the lower boundary of BB for the first time when $Z$ is examined upward in the upper part of BB starting from the BB peak. Marching upward, point A, the upper boundary, is defined where the

largest change in slope of $Z$ in the upper region of the BB. If A and B are the same, A is considered the top. However, if they are different, the upper boundary of the BB is whichever point is closest to the BB peak (Iguchi et al. 2016).

The top and bottom of the BB can also be determined using a DFR$_m$ method. The top is the height where the slope of the DFR$_m$ profile reaches a peak value. The bottom of the melting layer is where the DFR$_m$ profile has a local minimum (Le et al. 2016). A schematic is shown in Figure 13.
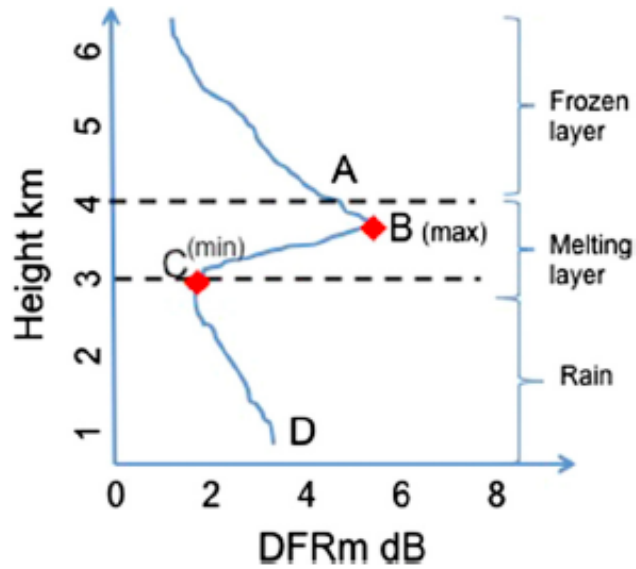


Figure 13: DFR$_m$ Example. Point A is where slope has peak value. Point B is local max. Point C is local minimum. Point D is DFR$_m$ closest to the surface (Figure 1 from Le et al. 2016).

To help distinguish between the different classifications of precipitation, some DFR$_m$ indices are defined. First, *V1* is

$$V1 = \frac{DFR_{ml}(\text{max}) - DFR_{ml}(\text{min})}{DFR_{ml}(\text{max}) + DFR_{ml}(\text{min})} \quad (10.)$$

where *DFR$_{ml}$* means DFR$_m$ in linear scale, DFR$_{ml}$(max) and DFR$_{ml}$(min) are linear values of DFR at points B and C, respectively, in Figure 12. Then let *V2* be

$$V2 = abs\big(mean(DFR_m slope)\big) \quad (11.)$$

$V2$ (dB km$^{-1}$) is the absolute value of the mean slope of DFR$_m$ below the local minimum point. Both V1 and V2 do not depend on the height or depth of the melting layer. $V1$ is typically larger for stratiform rain whereas $V2$ is larger for convective rain. However, to distinguish between the two types further, $V3$ is introduced as

$$V3 = \frac{V1}{V2} \quad (12.)$$

$V3$ provides a separable threshold to distinguish precipitation types. The precipitation is classified as convective for $V3 < 0.18$, stratiform for $V3 > 0.20$, and transition if between V3 falls between 0.18 and 0.20. These thresholds were calculated from 121 859 vertical profiles from 73 storms Integrated Precipitation and Hydrology Experiment and correspond to 70% of the cumulative density function (CDF) of $V3$ (Iguchi et al 2016). Figure 14 displays the flowchart of when the DFR$_m$ method is used for precipitation classification as compared to when the Ku-method is used. The single frequency method classifies rain into stratiform, convective, and other. Two methods are used to determine this. The vertical method detects stratiform first, meaning that the classification is stratiform if BB is detected. If BB is not detected, then the rain type is classified as convective is the radar reflectivity factors exceeds 39 dBZ or the storm top is greater than 15 km. For the horizontal method, the maximum radar reflectivity factor (Z$_{max}$) is used. If Z$_{max}$ exceeds a convective threshold or the pixel stands out from the surrounding area, the rain type of the convective center and adjacent pixels are convective. If Z$_{max}$ is not small enough to be noise, then it is stratiform. Else, the rain type is other (Iguchi et al. 2016).
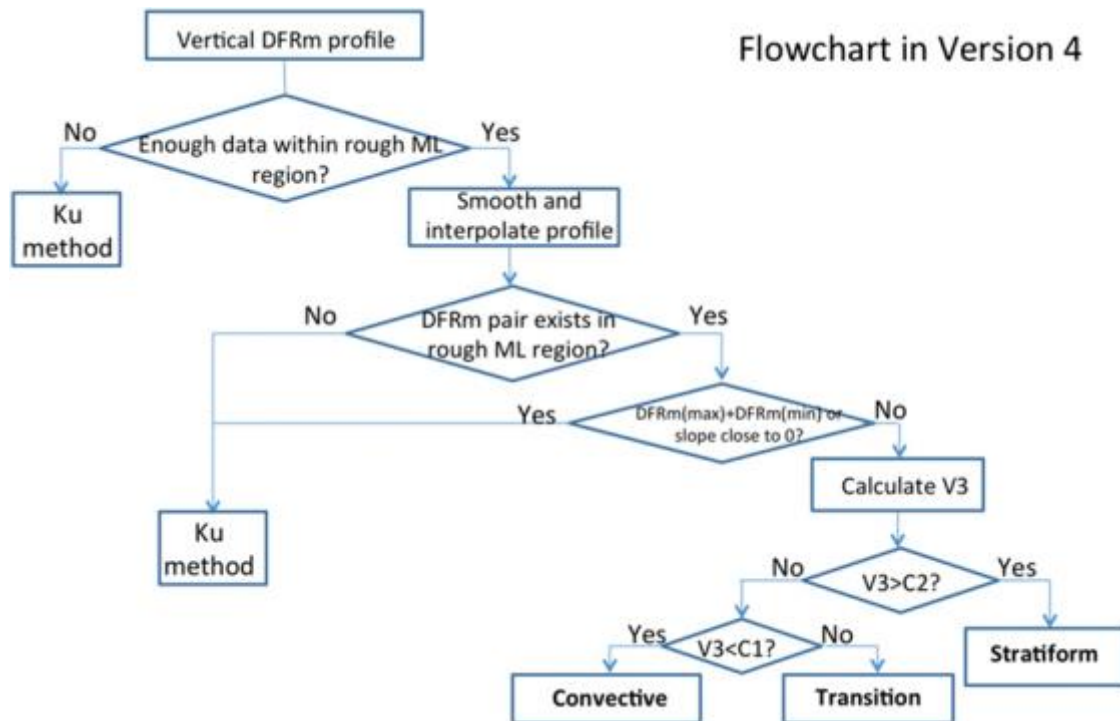
Figure 14. DFR$_m$ Flowchart. DFR$_m$ method flowchart for precipitation classification. Use of *V3* shown in bottom right portion of chart. (Figure 4 from Le et al. 2016)

In the DSD module, the phase of precipitation is determined for pixels with precipitation throughout the vertical column. The particle temperature is related to the dielectric constants which are dependent on the precipitation types and the detection of BB. Five range bins are assigned nodes A through E. In the case of stratiform precipitation with BB, the assignment of nodes is described in Table 3. For stratiform precipitation where BB was not detected, the process is the same except nodes B, C, and D are at the range bin corresponding to 0°C. This same process and node assignment is also used for convective precipitation and other-type precipitation. Phase is introduced, and if Phase is less than 100, then precipitation is solid and the particle temperature in Celsius is *Phase – 100*. Precipitation is liquid if Phase is 200-254 as 255 is saved for missing data. The particle temperature in Celsius for liquid can also be found, but the equation is *Phase – 200*. The range between 100 and 200 is for mixed-phase

precipitation but only values 125 – 175 are used. This range is used for intermediate positions as 100 represents the top of the bright band, 150 represents the peak of bright band, and 200 represents the bottom of the bright band (Iguchi 2016).

Table 3. Node Assignments. Description of node assignments for stratiform precipitation

Node A: Node A is the range bin with particle temperature closest to -20°C. At and above node A, precipitation is classified Solid.  Precipitation is Mixed if range bin is below node A and above node D.

Node B: Upper edge of BB. Above node B, particle temperate is ambient air temperature or is 0°C if air temperature is warmer than 0°C. Precipitation is Mixed.

Node C: Peak of BB. Between nodes B and D, particle temperature is set to 0°C. Precipitation is Mixed.

Node D:  Lower edge of BB. Below node D, particle temperature is also set to the ambient temperature, but is 0°C if air temperature is cooler than 0°C.  At and below node D, precipitation is Liquid.

Node E: Node E is the range bin with particle temperature closest to 20°C. Precipitation is Liquid.

CHAPTER III

METHODOLOGY

*a) Data*

The DPR data used was obtained from NASA's Precipitation Processing System (PPS) STORM database. The STORM database contains data for multiple satellites and is available to the public. There are two options to obtain data; PPS Data Access allows the user to customize their order and PPS Public Archive allows the user to obtain standard products via online ftp. For this study, PPS Data Access is used to obtain only parts of scans in the area of interest and request a customized selection of variables for storage efficiency. There are four levels of data (Level 0-3), but DPR is Level 2 which mostly consist of precipitation variables (STORM 2015). These data are used in this study. Two versions of data are used in this study. Version 4 was used for non-quality controlled data. During the work with non-quality controlled data, Version 5 was released. The reason two different versions of DPR data are used in this study is that the variables used to determine the quality of the data were not requested the first time data was ordered. Major changes in Version 5 are briefly discussed in Iguchi et al. (2017). These changes include redefining the transmitting powers, receiver's gains, beam widths, and pulse widths in the Level 1 data. This resulted in a change in reflective factor of +1.3 dB for KuPR and +1.2 dB for KaPR. In Level 2, adjustment factors were applied to the preparation module which resulted in a change to the measured received powers by a small fraction in dB. A DSD database was applied to the single frequency

31

algorithms so now precipitation estimates between the Ku-only and dual-frequency methods are in better agreement (JAXA 2017b).

Files requested were subset geographically and refined to a domain with points at 50°N, 24°N, 67°W, and 125°W. This means that selected files contained only parts of scans that occurred in that domain. This spatial area was chosen to include all ground stations (used for validation) in the Contiguous United States (CONUS). All files that met the spatial criteria and occurred from 15 March 2014 through 15 March 2016 were selected. The starting date of 15 March 2014 was selected because many of the early files soon after launch do not contain data. The last step in obtaining the data was to select parameters *phaseNearSurface* of the SLV module for the High Sensitivity Scan (HS), Matched Scan (MS), and Normal Scan (NS). Under the PREP variables, *binRealSurface* and *binClutterFreeBottom* were also selected to be used in a later calculation. *ScanTime*, which contains variables of date and time of each scan, and latitude and longitude were automatically included with each order.

Ground observation data is obtained from Iowa Environment Mesonet (IEM) database, which includes ASOS and AWOS ground stations. These were type of data used in Lott and Skofronick-Jackson (2017) and quality control of crowdsourcing data was a concern for a fair comparison. ASOS observations are reported hourly and at special times when significant weather is occurring whereas AWOS observations are reported typically every 20 minutes. All ASOS stations are equipped with precipitation instruments. Only certain types of AWOS stations can detect and determine the phase of precipitation. AWOS III stations are equipped with tipping bucket rain gauges. AWOS III P and AWOS III P/T stations are also equipped with tipping bucket rain gauges but additionally report the type of precipitation (All

32

Weather Inc. 2014). Observations were selected if they occurred within the same spatial and temporal constraints used for DPR data. Air Temperature (Fahrenheit), 1 Hour Precipitation (mm), and Present Weather as well as Latitude and Longitude of each station were requested for each observation. These observations follow the Federal Meteorological Handbook 1 (FMH1) which sets the standard on reporting weather conditions which can be automated, a human observation, or a combination of the two (U.S. DOC/NOAA 2005). For this study, FMH1 is used for determining Present Weather. Table 4 provides categories of Qualifiers and Weather Phenomena that are used to describe weather conditions in FMH1.

Table 4. Present Weather. Notations for reporting present weather in ground observations.
(Table 8-5 from U.S. DOC/NOAA 2005)

| QUALIFIER | | WEATHER PHENOMENA | | |
|---|---|---|---|---|
| INTENSITY OR PROXIMITY 1 | DESCRIPTOR 2 | PRECIPITATION 3 | OBSCURATION 4 | OTHER 5 |
| - Light<br>Moderate[2]<br>+ Heavy<br>VC In the Vicinity[3] | MI Shallow<br>PR Partial<br>BC Patches<br>DR Low Drifting<br>BL Blowing<br>SH Shower(s)<br>TS Thunderstorm<br>FZ Freezing | DZ Drizzle<br>RA Rain<br>SN Snow<br>SG Snow Grains<br>IC Ice Crystals<br>PL Ice Pellets<br>GR Hail<br>GS Small Hail and/or Snow Pellets<br>UP Unknown Precipitation | BR Mist<br>FG Fog<br>FU Smoke<br>VA Volcanic Ash<br>DU Widespread Dust<br>SA Sand<br>HZ Haze<br>PY Spray | PO Well-Developed Dust/Sand Whirls<br>SQ Squalls<br>FC Funnel Cloud Tornado Waterspout[4]<br>SS Sandstorm<br>DS Duststorm |

1. The weather groups shall be constructed by considering columns 1 to 5 in the table above in sequence, i.e., intensity, followed by description, followed by weather phenomena, e.g., heavy rain shower(s) is coded as +SHRA
2. To denote moderate intensity no entry or symbol is used.
3. See paragraph 8.4.1.a.(2), 8.5, and 8.5.1 for vicinity definitions.
4. Tornadoes and waterspouts shall be coded as +FC.

For FMH1, all present weather observations have an Intensity or Proximity Qualifier and

some may have a Descriptor. Weather Phenomena follow the Qualifier and it is possible for multiple phenomena to be present at once. If multiple Precipitation types are present, the most dominate is reported first followed by the other types in order of dominance (U.S. DOC/NOAA 2005).

*b)  Procedure*

Using the Federal Meteorological Handbook 1 as guidance, the FMH1 table was reduced by retaining only the necessary present weather notations. Certain parameters from Table 4 were used to create Table 5, which shows the observations that were compared with DPR phase measurements in this study. The following paragraphs explain the reason for reducing the FMH1 table.

Table 5. Present Weather Used. A revised Table 4 based on the Present Weather used in this study. Under the precipitation column, green and blue text indicates observations that were considered as liquid and solid, respectively.

| Qualifier | | Weather Phenomena | | |
|---|---|---|---|---|
| Intensity or Proximity | **Descriptor** | **Precipitation** | **Obscuration** | **Other** |
| +  **Heavy** <br> **Moderate** <br> -  **Light** | **BL**  Blowing <br> **SH**  Showers <br> **TS**  Thunderstorm <br> **FZ**  Freezing | **DZ**  Drizzle <br> **RA**  Rain <br> **SN**  Snow <br> **SG**  Snow Grains <br> **IG**  Ice Crystals <br> **PL**  Pellets <br> **GR**  Hail <br> **GS**  Small Hail | **BR**  Mist <br> **FG**  Fog <br> **HZ**  Haze | **Category not used** |

The Qualifiers VC (In the Vicinity), MI (Shallow), PR (Partial), BC (Patches), and DR (Low Drifting) were ignored. VC is used for weather phenomena occurring within 10 statute miles of, but not right at, the point of observation. MI, PR, and BC are only reported during fog, and DR is assigned to dust, sand, or snow being lifted less than 6 feet above the ground

by wind. BL (Blowing) was not ignored, as described in the following paragraph, as it is a common descriptor for snow and can occur while snow is falling.

The precipitation category was divided into solid and liquid phases. DZ (Drizzle) and RA (Rain) were classified as liquid. Everything else except UP (Unknown Precipitation) was classified as solid. UP was not included as it would be difficult to confirm the type of precipitation.  SN BLSN (Moderate Snow, Blowing Snow) , -SN BLSN (Light Snow, Blowing Snow), and  +SN BLSN (Heavy Snow, Blowing Snow) were also included in the solid types of precipitation. BR (Mist), FG (Fog), and HZ (Haze) were the only Obscurities included as these are more of a weather phenomenon than the others in this category.

Once the present weather categories were finalized, the next step was to compare the Global Precipitation Measurement (GPM) data with the ground observation data. Each GPM data file and ground observation file were matched by date. The minimum and maximum time (seconds of day in UTC) from GPM file is compared to the ground observation time, also in seconds of day and in UTC, to determine if either occurred within 1800 seconds (30 minutes) of each other. This was performed to quickly find observations that occurred during the scan period. ASOS stations report hourly and at special times if weather changes. If the weather does not change within the hour, then it is possible that a station is not included with a time constraint of less than 1800 seconds. As mentioned, GPM files are named by date, but the times of scans are in UTC. There were sections of scans over CONUS that started near the end of one day and completed during the next day. For example, a scan may start at 2355 UTC on Day 1 but complete at 0005 UTC on Day 2 and is named with the date of Day 2. The coordinating observation file , also named with the date of Day 2, starts at 0000 UTC and

ends at 2359 UTC. If these two files were compared, then observations at 2355 of Day 2 would be compared with DPR measurements of Day 1. To eliminate any possible issue with this, the minimum and maximum GPM time are also compared with each other. If this difference was less than an hour, then the scan occurred on the same day and would not cause any error comparing with observations that may have occurred the day before the end of the scan time. If these two criteria were met, then using the distance formula where

$$d = R * cos^{-1}(sin(lat_1)\,sin(lat_2) + \ cos(lat_1)\,cos(lat_2)\,cos(lon_1 - \ lon_2)) \quad (13.)$$

the distance between the location of the ground observation and each pixel of the GPM scan was calculated. If the shortest distance was less than 5 km, then the observation that occurred closest in time was taken as long as the difference between the two was still within 1800 seconds. Pixels of GPM Dual-frequency Precipitation Radar (DPR) are 5 by 5 km nadir, but pixels farther from nadir will be wider than 5 km. Using 5 km as the threshold guarantees that observations within the pixels farther from nadir will still be considered. If these criteria were met, then the observation was saved along with all other observations that also met the criteria for a particular GPM scan.

Despite many observations matching up with each GPM scan, it was common to have a station that reported more than once within the 1800 seconds. This was especially common with AWOS stations. In order to not count a station more than once, the observation with the smallest time difference compared to the scan time was selected from each ground station.

From this point, the present weather reported by the ground station and the phase near the surface as detected by DPR was compared. To display this comparison, the results were tallied in a Hit/Miss chart as shown below. If the GPM phase was consistent with

observations, then it was considered a "Hit" (shown along the diagonal).

Table 6. Hit/Miss. The Hit/Miss chart used to compare the observed present weather at the ground with the GPM phase measurements. The blue, purple, and red -shaded regions are used within the text examples (see main text). True positive (TP), False Positive (FP), and False Negative (FN) are shown for each type of precipitation (subscript s, m, or l for solid, mixed, or liquid, respectively). True Negative (TN) is also shown. Unfilled boxes represent where precipitation was detected but with inconsistent phase.

| | | DPR Phase Measurements (Test) | | | |
|---|---|---|---|---|---|
| | | **Solid** | **Mixed** | **Liquid** | **Nothing** |
| **Surface Present Weather Observation (Reference)** | **Solid** | $TP_s$ | | | $FN_s$ |
| | **Mixed** | | $TP_m$ | | $FN_m$ |
| | **Liquid** | | | $TP_l$ | $FN_l$ |
| | **Nothing** | $FP_s$ | $FP_m$ | $FP_l$ | TN |

Charts were generated for each month as well as for each case study. Cases are discussed in more detail later. There were two charts for each month as results were saved for eastern and western United States with the dividing line of 100°W longitude. This line was chosen because areas to the west are mainly mountainous, and a goal of this study was to investigate if the DPR's performance differed over highly, mountainous terrain. For this study, the Appalachian Mountains were not singled out as 'mountainous' as they cover only a small portion of eastern CONUS. All observation and GPM data that resulted in a hit were stored in a text file for each month. misses were stored in a separate file to be studied more in depth for certain case studies.

Using these data, a detection rate was calculated by taking the hits of one type of precipitation and dividing that by the total number of observations reporting the same precipitation. Then, focusing on only the occurrences DPR detected precipitation, the

percentage of correct classifications was calculated by taking the hits for a certain precipitation phase and dividing that by the total number of observations for that same phase when DPR also detected precipitation. These calculations are shown in the equations below:

$$Detection\ Rate = \frac{Hits(P)}{\Sigma\ Observations(P)} \quad (14.)$$

$$Detection\ Rate = \frac{Hits(P)}{\Sigma\ Observations\ GPM\ Detected(P)} \quad (15.)$$

where $P$ is the phase of interest. These two values were calculated for all scan modes and for liquid and solid precipitation whereas the latter was used to determine how well DPR performed at not detecting any precipitation when none was reported at the surface.

Adopting the methods used in Speirs et al. 2017, the probability of detection (POD), false alarm rate (FAR), and Heidke Skill Score (HSS) are calculated. Recall, POD is calculated using

$$POD = \frac{TP}{TP + FN} \quad (16.)$$

where $TP$ is the total number of true positives and $FN$ the total number of false negatives. True positive indicates when the test and reference both detect precipitation, in this case with DPR representing the test and ground observations representing the reference. Within the Hit/Miss table, the $TP$ and $FN$ counts for solid precipitation would be within the blue and purple box, respectively (Table 6). False positive (FP) is when precipitation is detected by the test but not by the reference. For solid precipitation, this is the red box in Table 6. FAR is calculated using

$$FAR = \frac{FP}{TP + FP} \quad (17.)$$

The Heidke Skill Score (HSS) or Cohen's Kappa is calculated using

$$HSS = \frac{2[TP(TN) - FP(FN)]}{(TP + FN)(FN + TN) + (TP + FP)(FP + TN)} \quad (18.)$$

where true negative, *TN,* represents the incidents of when both test and reference do not detect precipitation. In this study, the calculations for *TP* varied depending on the type of precipitation studied, and values for *FP* and *FN* depended on the method used for *TP*. *TP* was calculated four ways including two different ways for the 2-year results. The first was to calculate it across all the occurrences that DPR detected precipitation, whether it was correctly classified or not. The second method only included the hits of precipitation classification. Then POD, FAR, and HSS were calculated with *TP* values for solid as well as liquid precipitation.

Three major snow events (case studies) over the two-year period were chosen from the Weather Prediction Center's (WPC) archive of Storm Summaries based on location and the impacts of the event. Each case was studied using the same methods as stated above but with some slight differences as discussed further below. All possible scans covering each event were used and unlike the 2-year results, were not separated by east or west if there was overlap of 100°W longitude. The values of POD, FAR, and HSS were not calculated as they are insignificant for DPR's performance only for these few cases. These cases were used to study DPR's performance more in depth to determine where the misses occur relative to the event and what might be causing these errors. It is important to note that results from these scans may include nearby events that were not directly related to the case study, but happened to be in the scans used. This can be seen in the second case study and is discussed more in the results.

39

For case studies, the scan height relative to the lowest cloud deck was studied. The scan height can be found using

$$Lowest\ Clutter\ Free\ Bin = 125 * (binRealSurface - binClutterFreeBottom) \quad (19.)$$

where *Lowest Clutter Free Bin (LCFB)* is in meters and *binRealSurface* and *binClutterFreeBottom* are provided in the DPR L2 files and are part of the Preparation (PREP) Module. *binRealSurface* is the estimated surface position calculated from *echoPower* and level-1B products. *binClutterFreeBottom* is an estimate of range bin number of the clutter-free bottom using *echoPower* profiles and *binRealSurface* may be used as reference (Iguchi et al. 2016). The LCFB typically varies from 500 m (nadir) to as much as 2500 m (off nadir or in mountains) (personal communication, Joe Munchak, 2017). LFCB was only calculated for observations that reported a cloud deck. Taking the difference between LFCB and the lowest cloud deck, it can be determined if the scan was above or below cloud deck. If the difference is positive, then the scan occurred above the lowest cloud and is a possible explanation for incidents DPR did not correctly classify the detected precipitation. Henceforth, the term 'incidents' refers to the occurrences when there was an AWOS/ASOS observation that was comparable with a DPR point.

*c) Quality Control*

As discussed in the *Data* Section of this Chapter, the method above uses the Level 2 DPR data without looking at any of GPM's quality variables. Two quality variables were chosen from DPR: *qualityData* and *qualityFlag*. For the best data, these two variables should be equal to zero. If *qualityData* is any value other than zero, then there are errors in the data.

*qualityFlag* can vary from 0-2 and -99 for missing data, but zero represents high quality data (NASA 2014). These variables were not requested with the original, custom order of GPM data. The same variables were ordered again along with the quality variables. Between the time these two data sets were ordered, NASA/JAXA released Version 5 of the GPM data. Some files that were originally included in Version 4 were eliminated by JAXA for quality purposes. In other words, the original results come from Version 4, and the results with the quality variables included come from Version 5.

To compare this data with the ground observations, the method was the same except with the addition of the two data quality flags/variables. If both variables were zero (good quality data), then the DPR and ground observation points were compared. Hit/Miss charts were created using the new results. Probability of Detection, False Alarm Rate, and Heidke Skill Score were also calculated for this new data to compare with the data originally used. The terms "raw data" and "2-year data" will be used herein to describe the data that did not use the quality control variables. Also, the comparison between the two versions of DPR data is reasonable. The major changes discussed in the first section of this chapter should not have an influence on any of the variables used in this study. From the list provided by (NASA 2017e), none of the variables used in this study are listed as ones that were changed, meaning that the algorithms to calculate these were not changed. Some files that occurred soon after the launch of GPM were removed by JAXA due to the reliability of the data (Personal Communication, PPS Data Help Desk, 2017).

d) *Case Studies*

The winter storm of 29 January – 3 February 2015 that affected the upper Midwest and most of the Northeast was record making for many locations. This storm system originated in the southwest and over the span of just under a week, moved to the northeast. In its path, it left historic snowfall in major cities like Chicago, Detroit, and Boston. At least 3,000 flights were canceled and over half of those were in the Chicago area. The snow started in Colorado and New Mexico as the system was provided moisture from southwesterly flow creating a low-pressure system in Colorado with the upper level low in Montana. These two lows moved across the Great Plains and Midwest and the surface low strengthened. A strong southerly jet brought moisture to the system in the Ohio River Valley and easterly flow helped enhance snowfall totals in this area. As the system traveled to the northeast, it quickly strengthened and a second low developed near the Delmarva Peninsula. Warm, moist air over the Atlantic was forced over the front enhancing the snowfall totals in the northeast (Krekeler 2015). An overview of the low-pressure evolution for this event is shown in Figure 15. The 72-hour snowfall accumulation created by the National Operational Hydrologic Remote Sensing Center (NOHRSC) is displayed in Figure 16.
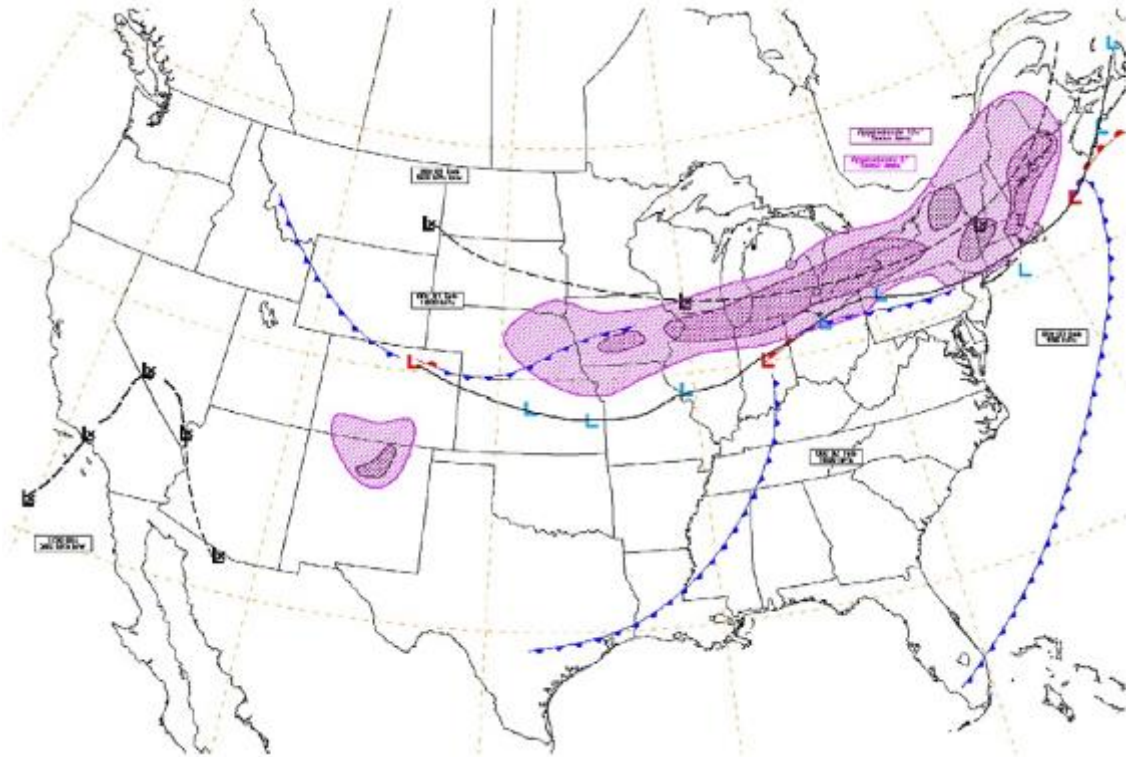
Figure. 15. 29 January –  3 February 2015 Case Study Weather Map. The setup and snow totals of the 29 January –  3 February 2015 snowstorm. 500 hPa lows are black with tracks denoted with black, dashed line and surface lows are red  and light blue with tracks denoted as black solid line. Light shade areas are regions of 6" snowfall and darker shaded areas represent regions of 12" snowfall. (Figure 1 from Krekeler 2015).
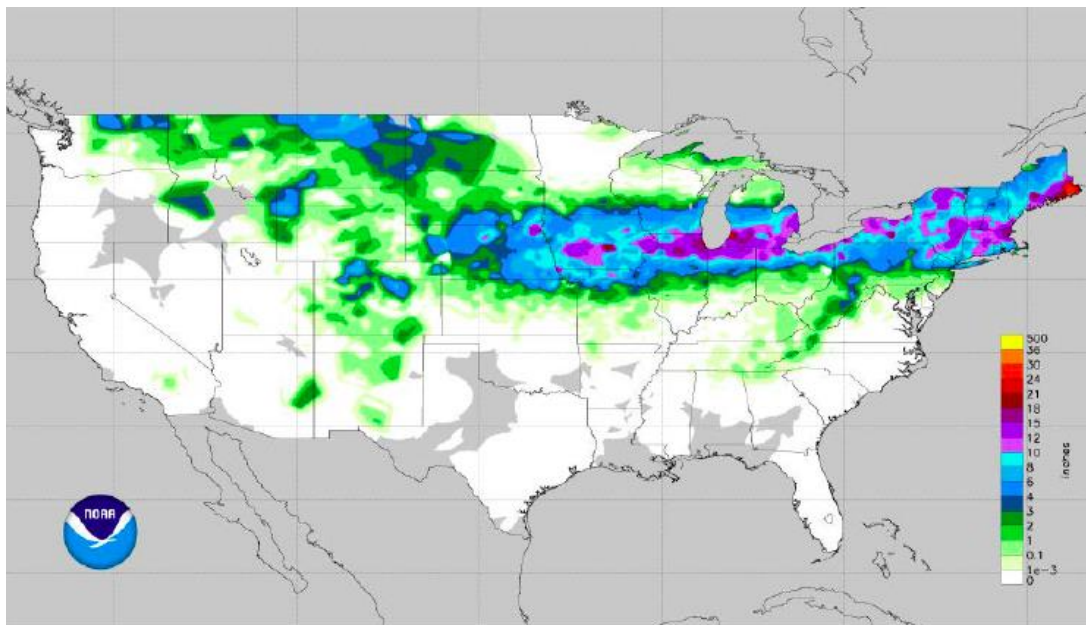


Figure 16. 29 January –  3 February 2015 Case Study Snowfall.  Color-filled contours of 72-

43

hour accumulation from the NOHRSC Snowfall Analysis ending at 12 UTC on 3 February 2015. (Figure 2 from Krekeler 2015.)

The second case study was selected to be the deadly 16-17 February 2015 Southern Plains and Mid-Atlantic winter storm. This storm contained a mixture of conditions including heavy snow, ice, and freezing temperatures, which resulted in poor road conditions and power outages. Parts of Kentucky, West Virginia, and Virginia received 12 to 20 inches of snow with 18 inches officially reported in Coleman, Kentucky. Three inches of sleet was recorded in Union City, Tennessee, and Strawberry Fields, Tennessee had the highest recorded freezing rain total of 0.75 inches. Over 300,00 power outages were reported in 14 states and the District of Columbia. Affecting more than 47 million people, governors in several states declared state of emergency. Schools and businesses were closed both days of the event. A woman got lost in the woods in Kentucky and died of hyperthermia. Another ten deaths were indirectly related to the storm system (Krekeler 2015).

Starting around 12 UTC on 16 February, there was an upper-level shortwave moving across the Plains after originating in the central Rockies. A surface low was present in Texas with a strong mid-level baroclinic zone just to the east. Strong, moist southerly flow from the Gulf of Mexico interacted with this zone creating wintry precipitation in the southern Plains. While snow fell mainly north of the surface low and frontal zone, sleet and freezing rain fell along the boundary. This occurred as the system continued to move across the northern Gulf States, and the baroclinic zone moved northeastward bringing heavy snow in the Mississippi and Tennessee/Ohio Valleys. This event tapered off early in the morning of 17 February as it moved off the Atlantic coast (Santorelli 2015). An overview of this storm is displayed in Figure 17. The 72-hour accumulated snowfall on 18 February 2015 at 12 UTC is displayed in

Figure 18.  From the two figures, Kentucky and West Virginia were the main locations of the

heaviest snowfall.
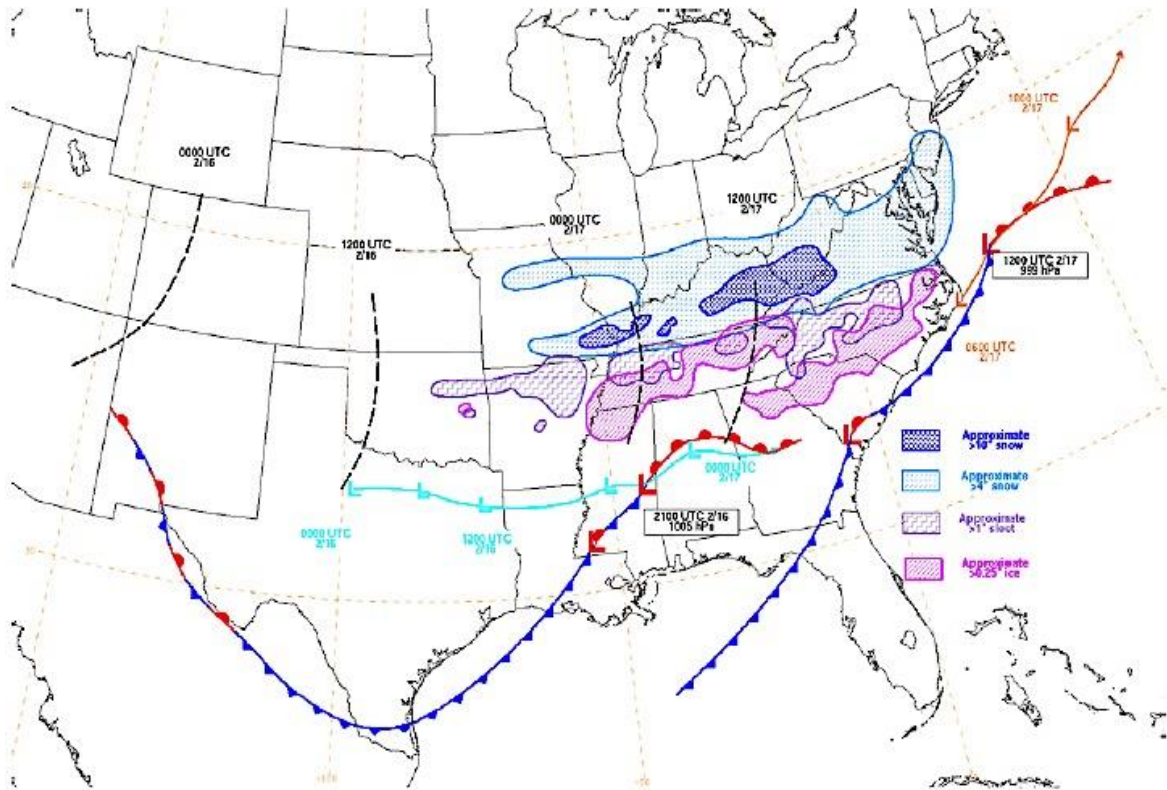


Figure 17: 16-17 February  2015 Case Study Weather Map. The setup and precipitation of the 16-17 February system. Black dashed lines indicate the 500 hPa shortwave trough. The surface lows are in red and orange. Areas of significant snow are shaded in blue with higher amounts represented by darker shades. Areas indicated by the purple, zig-zag shade represent areas that received more than an inch of sleet. The pink, dashed shaded areas are locations that received over 0.25 inches of ice. (Figure 2 Santorelli 2015)
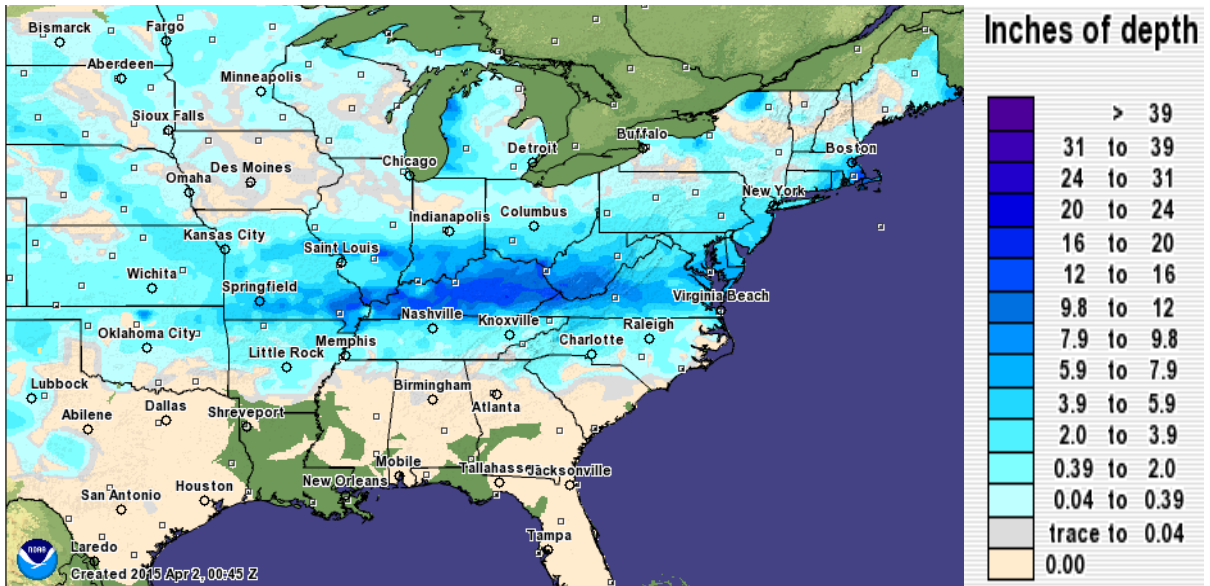
Figure 18. 16-17 February 2015 Case Study Snowfall. NOHRSC interpolated 72 hour observed snowfall analysis as of 12 UTC on 18 February 2015 (NOHRSC 2017).

The 17-18 November 2017 storm provided snow and rain for many areas. The heaviest snowfall occurred in the higher elevations of the southern Rockies. Blizzard conditions occurred with the snow forcing the cancellations of flights and closures of interstate highways (Krekeler 2016). Colorado Springs received 16 inches of snow. Heavy snow also fell in parts of Kansas with 20 inches observed in Colby. Snow was also observed in parts of Nebraska, Oklahoma, and Texas. Rain was observed from the Central/Southern Plains to the Southeast with most areas receiving a few inches but others received 5+ inches (WPC 2015). The 48-hour snowfall accumulation can be seen in Figure 19.
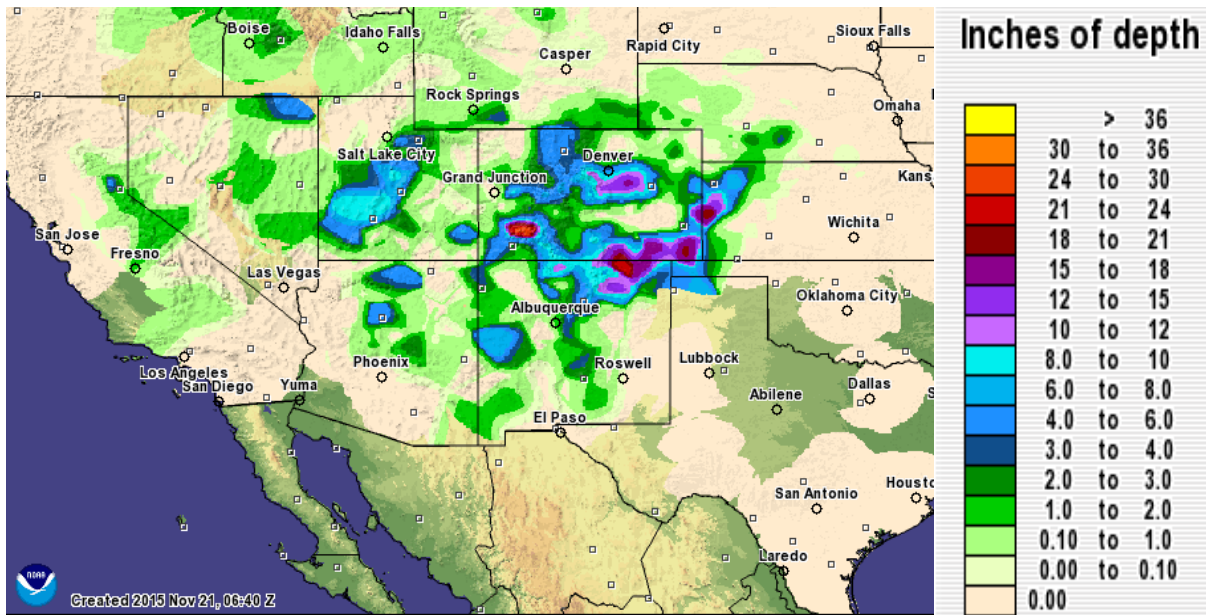
Figure 19. 16-18 November 2015 Case Study Snowfall. NOHRSC interpolated 48 hour observed snowfall analysis as of 00 UTC on 18 November 2015 (NOHRSC).

This event, summarized in Figure 20, started on 16 November with a 500 hPa trough centered over Nevada and a southwesterly jet at 300 hPa over the Four Corners with divergent upper-level flow over the areas that received the heavy snowfall. By 0000 UTC on the 17th, the 500 hPa low had deepened and centered over the Four Corners region. Lifting from a strong 700 hPa jet over parts of southern Colorado and New Mexico favored the southwest-facing slopes for the heaviest snowfall. By 12 UTC, the 500 hPa low had moved centering itself over the Panhandle of Texas. In result, the upslope flow and heavy snow shifted to the eastern side of the Rockies. A strong 850 hPa front and moisture from the southeast supported an additional band of heavy snow in western Kansas (Krekeler 2016). This system moved eastward and the surface low was observed west of Minneapolis the morning of the 18th. An occluded front extended from the low through the Illinois/Tennessee Valley with the cold front stretching from there down to Mississippi and Alabama. A warm

front extended from where the other two fronts met (triple point) trough Alabama and Georgia. This system moved to the coast by the evening of 19 November. Due to the heavy rainfall affecting many areas, flash flood watches, warnings, and advisories were issued throughout the duration of this system (WPC 2015).
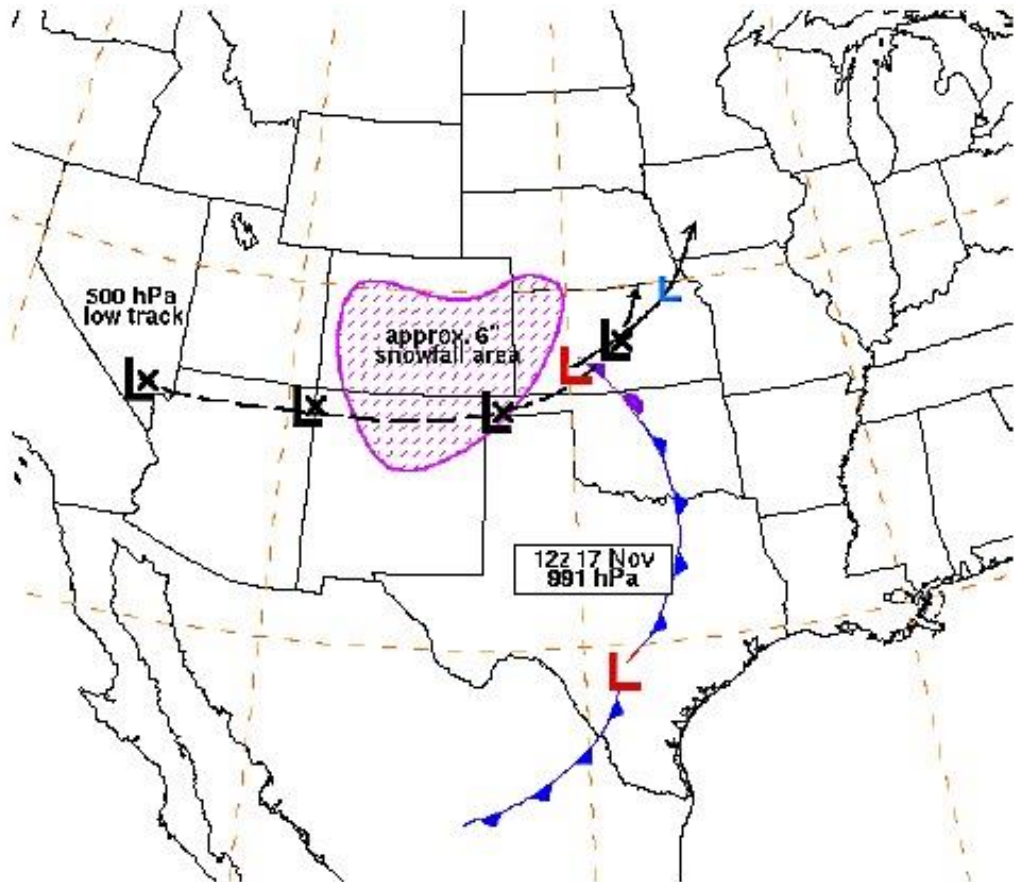


Figure 20. 16-18 November 2015 Case Study Weather Map. The setup and snowfall of the 16-18 November 2015 system. The black 'L' and lines indicate the 500 hPa low position and tracks. Red 'L' indicates surface lows with surface fronts also plotted. The pink shaded area is the approximate area receiving at least 6 inches of snowfall (Kreckler 2016).

CHAPTER IV

RESULTS

*a) 2-Year Results*

The results show that the Dual-frequency Precipitation Radar (DPR) on the Global
Precipitation Measurement (GPM) Core Observatory satellite does fulfill the requirement to
detect snow/solid precipitation, but there is room for improvement in future measurements or
revised algorithms. Comparing the ground observations with the DPR measurements shows
that the solid precipitation detection rate, calculated from Tables 7-9, is quite poor, resulting
in 20.6%, 20.9% and 17.8% for High Sensitivity Scan (HS), Matched Scan (MS), and
Normal Scan (NS) respectively in the east. In the west, these percentages are lower at 14.4%,
14.2%, and 12.8% respectively. These values are displayed in Figure 21. It only does slightly
better in HS mode than MS mode. Considering only correctly-detected solid precipitation
(blue box, Table 6) and ignoring the misses, DPR, classification results are significantly
better compared to the detection rate. For all three scans in the east, assuming any detection
was given, the rate that DPR correctly classified solid phase, when there were solid phase
ground measurements, was around 96%. All scans in the west performed slightly better with
a correct classification rate of about 98%. There were no occurrences of DPR correctly
classifying mixed phase precipitation. However, there were not enough mixed phase
precipitation ground observations to be able to make significant conclusions if there had been
matches.
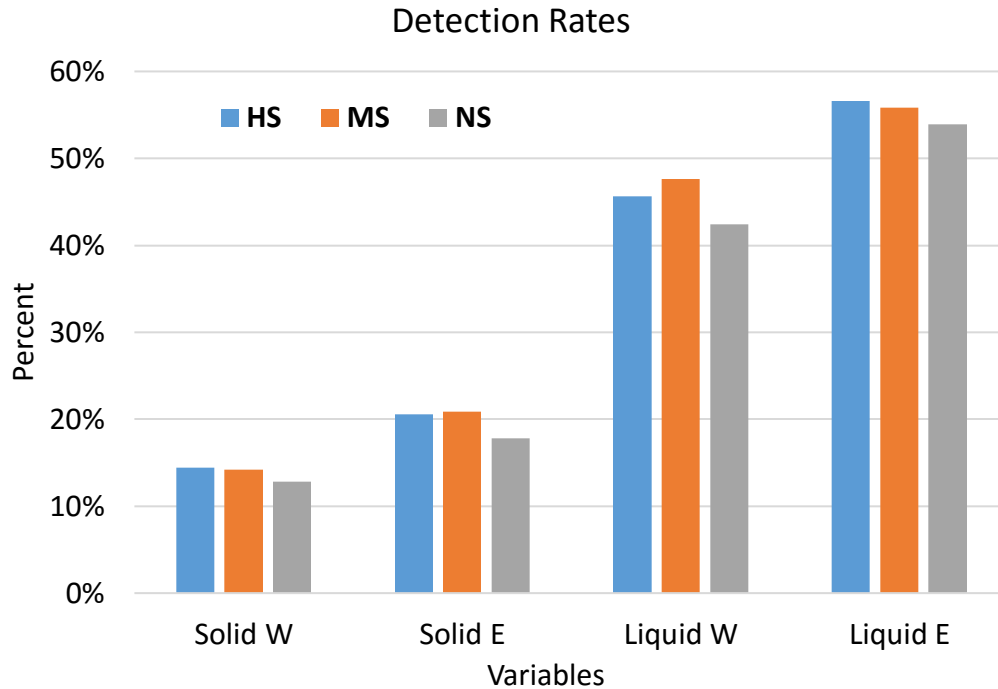
Detection Rates



Figure 21. Detection Rates. The detection rates of solid and liquid precipitation in the west and east for all three scan modes: High Sensitivity Scan, Matched Scan, and Normal Scan.

Table 7: HS Hit/Miss. Hit/Miss chart HS west and east of 100°W. Matches are along the diagonals.

| | | DPR HS Scan West | | | | DPR HS Scan East | | | |
|---|---|---|---|---|---|---|---|---|---|
| | | **Solid** | **Mixed** | **Liquid** | **Nothing** | **Solid** | **Mixed** | **Liquid** | **Nothing** |
| **Surface Present Weather Observation** | **Solid** | 104 | 0 | 2 | 615 | 486 | 0 | 18 | 1847 |
| | **Mixed** | 2 | 0 | 0 | 5 | 7 | 0 | 6 | 10 |
| | **Liquid** | 169 | 0 | 758 | 734 | 276 | 0 | 4082 | 2852 |
| | **Nothing** | 216 | 0 | 787 | 49759 | 422 | 0 | 2904 | 132741 |

Table 8: MS Hit/Miss Hit/Miss chart MS west and east of 100°W. Matches are along the diagonals.

| | | DPR MS Scan West | | | | DPR MS Scan East | | | |
|---|---|---|---|---|---|---|---|---|---|
| | | **Solid** | **Mixed** | **Liquid** | **Nothing** | **Solid** | **Mixed** | **Liquid** | **Nothing** |
| **Surface Present** | **Solid** | 106 | 0 | 2 | 640 | 510 | 0 | 21 | 1910 |

| Weather Observation | Table 8 continued | | | | | | | |
|---|---|---|---|---|---|---|---|---|
| | **Mixed** | 1 | 0 | 0 | 6 | 5 | 0 | 4 | 14 |
| | **Liquid** | 150 | 0 | 821 | 753 | 251 | 0 | 4187 | 3063 |
| | **Nothing** | 180 | 0 | 848 | 51803 | 430 | 0 | 2768 | 138211 |

Table 9: NS Hit/Miss. Hit/Miss chart NS west and east of 100°W. Matches are along the diagonals.

| | | DPR NS Scan West | | | | DPR NS Scan East | | | |
|---|---|---|---|---|---|---|---|---|---|
| | | **Solid** | **Mixed** | **Liquid** | **Nothing** | **Solid** | **Mixed** | **Liquid** | **Nothing** |
| **Surface Present Weather Observation** | **Solid** | 180 | 0 | 3 | 1219 | 867 | 0 | 38 | 3959 |
| | **Mixed** | 2 | 0 | 1 | 9 | 9 | 0 | 6 | 24 |
| | **Liquid** | 376 | 0 | 1437 | 1570 | 599 | 0 | 8063 | 6301 |
| | **Nothing** | 419 | 0 | 1387 | 102553 | 825 | 0 | 5380 | 273011 |

Recall that GPM-CO is the second satellite in history equipped with a radar (DPR) to measure rainfall. DPR does a better job at correctly classifying solid precipitation than it does liquid. For HS, MS, and NS modes in the eastern area, the detection rate for liquid precipitation was 56.6%, 55.8%, and 53.9% respectively. Just like with solid phase precipitation, DPR struggles to correctly detect liquid precipitation in the west, mostly due to missed detections, but also because of misidentifying it as solid precipitation. For the three scans, the percentages of correctly detecting liquid precipitation in the western area decrease to 45.6%, 47.6% and 42.4% respectively. Again, focusing on the instances of when DPR detects any precipitation and correctly classifies it (TP cells in Table 6), the result is different from solid precipitation. In the east, all scans do well correctly classifying liquid phase

precipitation at around 93-94%. The results from the west do not show the same consistency. The MS does the best with a correct rate of about 85% and HS is slightly behind with 82%. However, this value decreases to 79% for NS. Thus, DPR algorithm appears to over-detect precipitating ice when it is really precipitating liquid water.

Besides studying how well DPR detects and correctly classifies precipitation, it was worth studying how it performs at not detecting anything (True Negatives). For the majority of incidents in Tables 7-9, the satellite and ground observations match when no precipitation is measured. However, there were also false detections of precipitation when nothing was observed at the ground.

Table 10. HS Stats. 2-year results of probability of detection (POD), false alarm rate (FAR), and Heidke Skill Score (HSS) of the HS mode for both west and east. POD and FAR are in hundreds of percent.

|  | HS West | | | | HS East | | | |
|---|---|---|---|---|---|---|---|---|
|  | All | Hits | Solid | Liquid | All | Hits | Solid | Liquid |
| POD | 0.433 | 0.389 | 0.145 | 0.508 | 0.509 | 0.492 | 0.208 | 0.589 |
| FAR | 0.492 | 0.538 | 0.675 | 0.509 | 0.406 | 0.421 | 0.465 | 0.416 |
| HSS | 0.445 | 0.399 | 0.193 | 0.484 | 0.519 | 0.503 | 0.293 | 0.565 |

Table 11. MS Stats. 2-year results of probability of detection (POD), false alarm rate (FAR), and Heidke Skill Score (HSS) of the MS mode for both west and east. POD and FAR are in hundreds of percent.

|  | MS West | | | | MS East | | | |
|---|---|---|---|---|---|---|---|---|
|  | All | Hits | Solid | Liquid | All | Hits | Solid | Liquid |
| POD | 0.436 | 0.399 | 0.142 | 0.522 | 0.500 | 0.485 | 0.211 | 0.578 |
| FAR | 0.488 | 0.526 | 0.629 | 0.508 | 0.391 | 0.405 | 0.457 | 0.398 |

| Table 11 continued | | | | | | | | |
|---|---|---|---|---|---|---|---|---|
| HSS | 0.448 | 0.410 | 0.199 | 0.491 | 0.520 | 0.506 | 0.297 | 0.569 |

Table 12: NS Stats. 2-year results of probability of detection (POD), false alarm rate (FAR), and Heidke Skill Score (HSS) of the NS mode for both west and east. POD and FAR are in hundreds of percent.

| | NS West | | | | NS East | | | |
|---|---|---|---|---|---|---|---|---|
| | All | Hits | Solid | Liquid | All | Hits | Solid | Liquid |
| POD | 0.417 | 0.366 | 0.129 | 0.478 | 0.482 | 0.465 | 0.180 | 0.561 |
| FAR | 0.475 | 0.528 | 0.699 | 0.491 | 0.393 | 0.410 | 0.488 | 0.400 |
| HSS | 0.443 | 0.391 | 0.174 | 0.479 | 0.509 | 0.491 | 0.259 | 0.559 |

Glancing over tables 10-12, it easy to see that for all scan modes, the DPR performed better in the east. Compared to the previous results discussed earlier from this study, this was expected. In the west, the POD of DPR detecting any precipitation is at least 40%. This value decreases when calculated for the incidents when the phase of precipitation was correctly classified. The false alarm rates for both categories hover around 50%. For solid precipitation, the POD is less than 15% for all three scan modes and FAR is quite high. Due to these results, it is not surprising that the HSS for solid precipitation is low with values less than 0.2. Examining the liquid precipitation results, each category is better than the overall result. The POD is higher while FAR is lower.

As mentioned, the results in over the eastern region are better. Looking at all precipitation, POD is around 50% and the hits are close to 50% as well. The FAR decreases across all scan modes compared to the west. Focusing again on solid precipitation, the PODs

53

improve to over 20% and FAR drops below 50%. These help improve the value of HSS as well. There was better performance with liquid precipitation with POD increasing by at least 5%. FAR is below 40% for all three scan modes. In the west, HSS values were around 0.48, but increases to around 0.56 across all scan modes. The results for liquid precipitation in the east were overall the best.

*b) Quality Control Results*

The results from adding in the quality variables are shown in Tables 13-15. The first finding that stands out is the difference in values between the quality controlled data and the non-quality controlled data of when DPR did not detect precipitation when there was precipitation reported on the surface. This should be expected as discussed earlier in Chapter 2, level-2 values would be overwritten as missing data if *dataQuality* was not zero. The rate of detecting solid precipitation in the east for the High Sensitivity Scan at was 20.6%. For Matched and Normal scans, this was 21.7% and 18.8%, respectively. In the west, there were changes for all three scans with values of 16.7%, 16.8%, and 14.1% for HS, MS, and NS, respectively. The correct classification rates remained the same at around 96% for the east and 98% for the west.

Table 13. QC HS Hit/Miss. The Hit/Miss chart of HS for west and east of 100°W using the quality variables as criteria. Matches are along the diagonals. QC (quality control) is used to distinguish between the raw data and the quality controlled data

| | | QC DPR HS Scan West | | | | QC DPR HS Scan East | | | |
|---|---|---|---|---|---|---|---|---|---|
| | | Solid | Mixed | Liquid | Nothing | Solid | Mixed | Liquid | Nothing |
| **Surface Present Weather Observation** | **Solid** | 102 | 0 | 2 | 610 | 478 | 0 | 17 | 1824 |
| | **Mixed** | 2 | 0 | 0 | 5 | 6 | 0 | 6 | 10 |

| | Solid | Mixed | Liquid | Nothing | Solid | Mixed | Liquid | Nothing |
|---|---|---|---|---|---|---|---|---|
| **Liquid** | 171 | 0 | 738 | 719 | 267 | 0 | 4061 | 2727 |
| **Nothing** | 213 | 0 | 762 | 49082 | 414 | 0 | 2897 | 130492 |

Table 14: QC MS Hit/Miss. The Hit/Miss chart of MS for west and east of 100°W using the quality variables as criteria. Matches are along the diagonals. QC (quality control) is used to distinguish between the raw data and the quality controlled data

| | | QC DPR MS Scan West | | | | QC DPR MS Scan East | | | |
|---|---|---|---|---|---|---|---|---|---|
| | | Solid | Mixed | Liquid | Nothing | Solid | Mixed | Liquid | Nothing |
| **Surface Present Weather Observation** | **Solid** | 124 | 0 | 3 | 611 | 524 | 0 | 21 | 1870 |
| | **Mixed** | 1 | 0 | 0 | 6 | 5 | 0 | 5 | 12 |
| | **Liquid** | 161 | 0 | 825 | 708 | 257 | 0 | 4245 | 2835 |
| | **Nothing** | 191 | 0 | 876 | 51021 | 472 | 0 | 2981 | 135714 |

Table 15: QC NS Hit/Miss. The Hit/Miss chart of NS for west and east of 100°W using the quality variables as criteria. Matches are along the diagonals. QC (quality control) is used to distinguish between the raw data and the quality controlled data.

| | | QC DPR NS Scan West | | | | QC DPR NS Scan East | | | |
|---|---|---|---|---|---|---|---|---|---|
| | | Solid | Mixed | Liquid | Nothing | Solid | Mixed | Liquid | Nothing |
| **Surface Present Weather Observation** | **Solid** | 195 | 0 | 3 | 1187 | 903 | 0 | 38 | 3859 |
| | **Mixed** | 2 | 0 | 1 | 9 | 10 | 0 | 7 | 21 |
| | **Liquid** | 401 | 0 | 1430 | 1476 | 610 | 0 | 8177 | 5801 |
| | **Nothing** | 453 | 0 | 1470 | 100537 | 907 | 0 | 5720 | 266889 |

For the correctly detecting rainfall, the values are 57.6%, 57.9%, and 56.1% for HS, MS, and NS modes, respectively in the east. As determined before, these values are lower in the

west at 45.3%, 48.7%, 43.2%. The new detection rates along with the 2-year detection rates from Figure 21 are displayed in Figure 22.

**Detection Rates with QC**
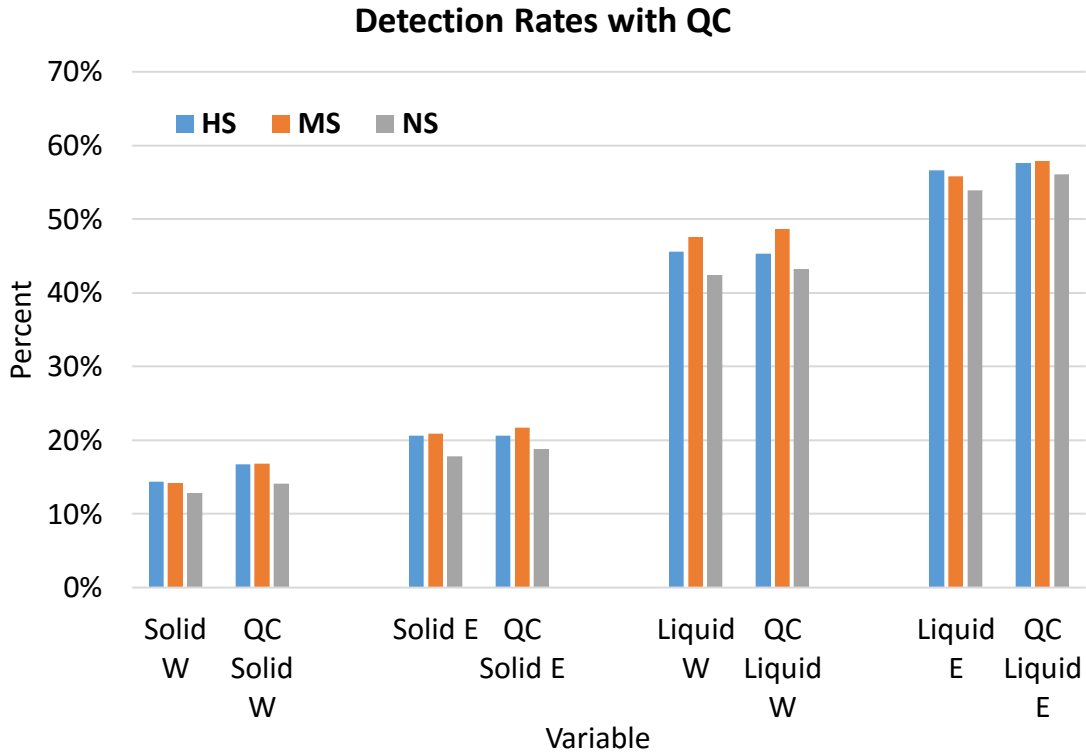


Figure 22. QC Detection Rates. The detection rates of solid and liquid precipitation in the west and east for all three scan modes: High Sensitivity Scan, Matched Scan, and Normal Scan. The quality controlled and 2-year results are both shown.

With the new data, all scans show 93-94% correct classification rates as shown previously. However, when calculating the same values in the west, a slight change is observed. Originally, the rates in the west were around 82%, 85%, and 79% for HS, MS, and NS, respectively, but the new results put these values around 81%, 84%, and 78%, respectively. All three scans stay consistent in agreement with ground observations when nothing is observed. Hit/Miss charts were also created with the new data for the case studies, but there were no significant changes to show from those results. In fact, nothing changed in the HS Hit/Miss charts in all three case studies.

56

Changes are observed in the new quality-controlled probability of detection, false alarm rate, and Heidke Skill Score values. These new values are shown in Tables 16-18. Focusing on the west first, changes are shown in all three metrics. The reason for these changes might be due to a smaller sampling size in the quality controlled results compared to the original 2-year totals. For MS and NS, there are improvements in for all calculations of POD for the western area. The FAR does not change much for MS and NS. The skill score improves for these as well except for the hits in NS.

Table 16. QC HS Stats. 2-year results of probability of detection (POD), false alarm rate (FAR), and Heidke Skill Score (HSS) of the HS mode for both west and east for the quality controlled data. POD and FAR are in hundreds of percent.

|  | QC HS West | | | | QC HS East | | | |
|---|---|---|---|---|---|---|---|---|
|  | All | Hits | Solid | Liquid | All | Hits | Solid | Liquid |
| POD | 0.432 | 0.386 | 0.143 | 0.507 | 0.515 | 0.499 | 0.208 | 0.598 |
| FAR | 0.490 | 0.537 | 0.676 | 0.508 | 0.406 | 0.422 | 0.464 | 0.416 |
| HSS | 0.445 | 0.398 | 0.192 | 0.484 | 0.522 | 0.506 | 0.292 | 0.570 |

Table 17. QC MS Stats. 2-year results of probability of detection (POD), false alarm rate (FAR), and Heidke Skill Score (HSS) of the MS mode for both west and east for the quality controlled data. POD and FAR are in hundreds of percent.

|  | QC MS West | | | | QC MS East | | | |
|---|---|---|---|---|---|---|---|---|
|  | All | Hits | Solid | Liquid | All | Hits | Solid | Liquid |
| POD | 0.457 | 0.417 | 0.169 | 0.538 | 0.517 | 0.503 | 0.219 | 0.600 |
| FAR | 0.489 | 0.529 | 0.606 | 0.515 | 0.406 | 0.420 | 0.474 | 0.413 |
| HSS | 0.459 | 0.420 | 0.230 | 0.495 | 0.524 | 0.510 | 0.302 | 0.572 |

Table 18. QC NS Stats. 2-year results of probability of detection (POD), false alarm rate (FAR), and Heidke Skill Score (HSS) of the NS mode for both west and east for the quality controlled data. POD and FAR are in hundreds of percent.

| | QC NS West | | | | QC NS East | | | |
|---|---|---|---|---|---|---|---|---|
| | All | Hits | Solid | Liquid | All | Hits | Solid | Liquid |
| POD | 0.432 | 0.378 | 0.141 | 0.492 | 0.502 | 0.484 | 0.190 | 0.585 |
| FAR | 0.486 | 0.542 | 0.699 | 0.507 | 0.405 | 0.422 | 0.501 | 0.412 |
| HSS | 0.447 | 0.292 | 0.185 | 0.478 | 0.515 | 0.497 | 0.268 | 0.566 |

The POD in the eastern area for all scans and all methods of calculation increases with one exception when the HS mode has a slight decrease for solid precipitation when compared with the 2-year values. The same is true for the western areas except there was no change in HS mode for solid precipitation. The FAR stays relatively the same across the board for both areas for HS. However, an increase in FAR is observed for MS and NS modes for all categories. Despite this, the HSS increased for all scans and all calculations except for solid precipitation in HS mode. Overall, the new results show improvements in performance when eliminating bad data.

*c) 29 January – 3 February 2015 Winter Storm*

The first thing that stands out in this case is how similar the results are between the High Sensitivity Scan (HS) and Matched Scan (MS), as seen in Table 19. This is not the case for the 2-year results, but they are similar on smaller time scales due to their similar scan widths. However, looking more closely, the HS has less misses than MS, especially when it

determined there was not precipitation even though there was precipitation observed at the ground. When all scans detect precipitation, they all correctly classify solid precipitation. Despite this, all are missing a large portion of these incidents. As expected HS detected 61.5% of these incidents, but MS was close as well with 58%. NS performed the worse at detecting 42.9% of the solid precipitation incidents. As mentioned, the scans did not perform as well with liquid precipitation. Normal Scan (NS) performed the best of the three scans with catching 43.5% of these incidents. MS and HS are not far behind with detection success of around 40%. For this storm, all scans perform better at detecting solid precipitation but worse at detecting liquid precipitation compared to the 2-year results. In the incidents when no precipitation was observed at the ground, the scans do well with detection rates over 90%.

Table 19: 29 January – 3 February 2015 Case Study Hit/Miss. Hit/Miss chart for 29 January – 3 February 2015 winter storm for HS, MS, and NS

| DPR HS | | | | | |
|---|---|---|---|---|---|
| | | **Solid** | **Mixed** | **Liquid** | **Nothing** |
| **Surface Present Weather Observation** | **Solid** | 48 | 0 | 0 | 30 |
| | **Mixed** | 0 | 0 | 0 | 1 |
| | **Liquid** | 19 | 0 | 26 | 19 |
| | **Nothing** | 7 | 0 | 12 | 190 |
| DPR MS | | | | | |
| | | **Solid** | **Mixed** | **Liquid** | **Nothing** |
| **Surface Present Weather Observation** | **Solid** | 47 | 0 | 0 | 34 |
| | **Mixed** | 0 | 0 | 0 | 1 |
| | **Liquid** | 14 | 0 | 27 | 28 |

| Table 19 continued | | | | |
|---|---|---|---|---|
| **Nothing** | 6 | 0 | 10 | 199 |
| **DPR NS** | | | | |
| | | **Solid** | **Mixed** | **Liquid** | **Nothing** |
| **Surface Present Weather Observation** | **Solid** | 69 | 0 | 0 | 92 |
| | **Mixed** | 0 | 0 | 0 | 1 |
| | **Liquid** | 23 | 0 | 47 | 54 |
| | **Nothing** | 9 | 0 | 13 | 424 |

Investigating the cases where DPR detected precipitation but nothing was reported at the ground, led to support that DPR may be performing better than the 2-year results show. For HS and NS, there were four solid and four liquid incidents when there was 'M' reported in the Present Weather category, but there were precipitation amounts recorded by those stations. MS had three of each event for the same situation. In most of the other incidents not accounted for in the numbers above, the ground station was either AWOS III, AWOS III P, or AWOS III P/T. These stations may not have been equipped with the needed instruments or the instruments were not working. Sampling a few of the stations around the scan time supports this theory as observations taken before and after the scan time did not report precipitation of any kind. Studying the liquid ground observations, when DPR HS and MS modes detected solid precipitation, the surface temperature, as measured by the station, was always above freezing. For NS, this was also true except for one station where the surface temperature was about -4°C.
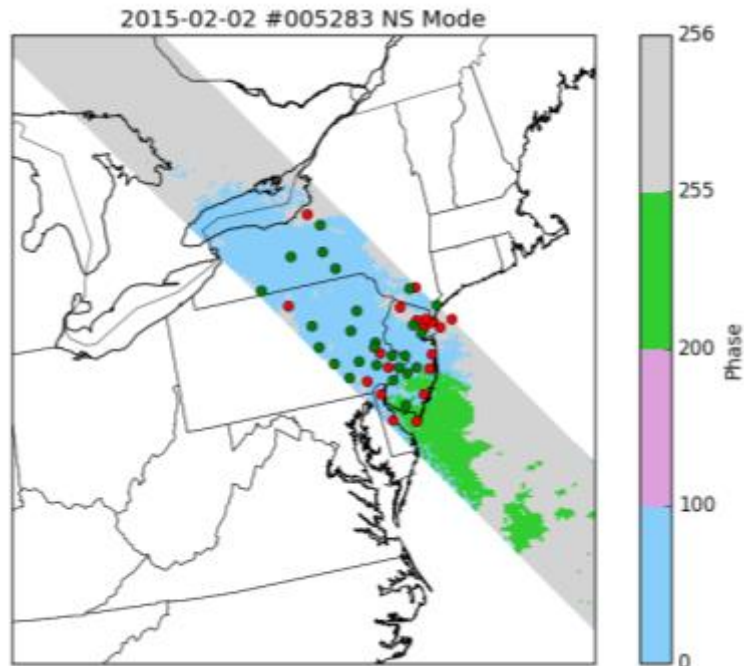
Figure 23.  Scan #005283. NS mode of phaseNearSurface from scan #005283 on 2 February 2015 at 0535-0542 UTC with solid (blue), liquid (green), and no precipitation (gray) along the swath path. Green dots indicate locations where ground observations and DPR agreed. Red dots are where they did not. Dots are not shown for when both do not detect any precipitation.

Figure 23 shows *phaseNearSurface* of NS mode from scan #005283 that passed over the Northeast on 2 February 2015 Scan #005383 was one of five scans used in this study, and Figure 24 shows the KDIX ground radar reflectivity for the results from GPM scan #005283. Scan #005283 was interesting because it shows an area of transition between snow and rain. This can be seen in Figure 25 as a stationary front is present just north of New Jersey. Most of the misses (red dots) occurred near this zone. This scan also had a dense area of observations available in a small portion of the scan. Beyond the transition zone, there are more hits (green dots) than misses visible in the solid precipitation region. Focusing on New Jersey, Figure 24 shows the misses that occurred in that area, and many of the misses involved DPR not detecting precipitation. The majority of those instances fall in areas of

61

reflectivity below the Minimum Detectable Signal (MDS), 18 dBZ, of DPR. There were also

a few instances where DPR detected precipitation but no Present Weather was reported. (red

triangles in Figure 24) Also shown in Figure 24 are the instances when DPR and ground

observations disagreed on the precipitation phase.
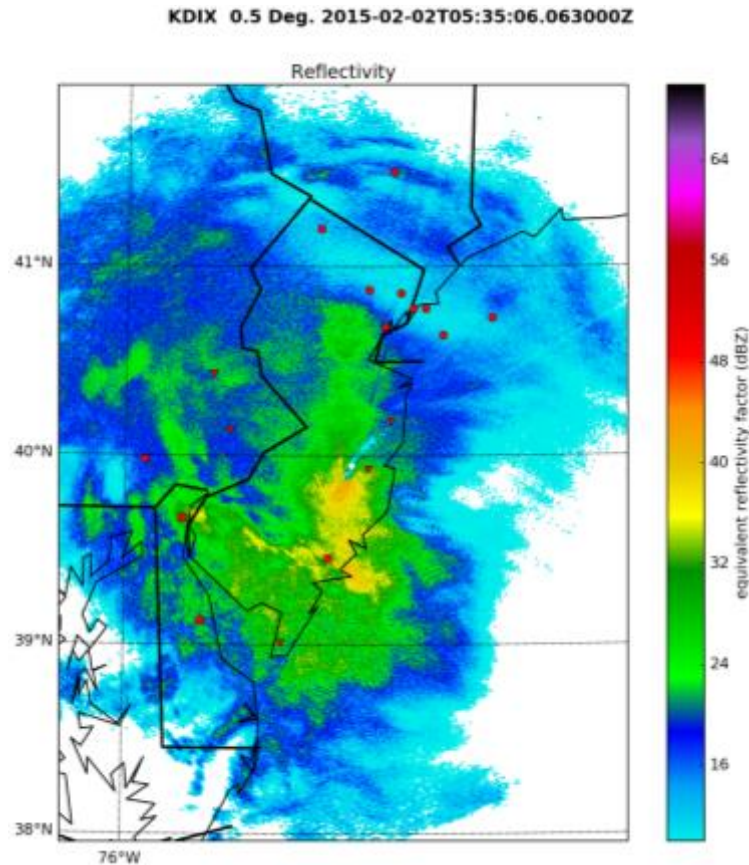


Figure 24. KDIX Radar. The reflectivity of the lowest scan of KDIX Radar on 2 February
2015 at 0535 UTC. Misses, based on the Normal Scan mode from GPM scan #005283 are
displayed with circles, triangles, and squares. Circles are the misses when DPR did not
detect any precipitation but ground observations did. Triangles represent the misses when
DPR did detect any precipitation but no Present Weather was reported by the ground
observation. Squares represent when both the ground observation and DPR reported a
precipitation phase but disagreed on the phase type (e.g. DPR reports solid, ground
observation reports liquid).

Figure 25. 2 February Surface Map. Daily surface map the morning of 2 February 2015 valid at 7 am Eastern Time. Area of precipitation shaded in green. Note the area of precipitation in the northeast where scan #005283 took place (DOC 2017).
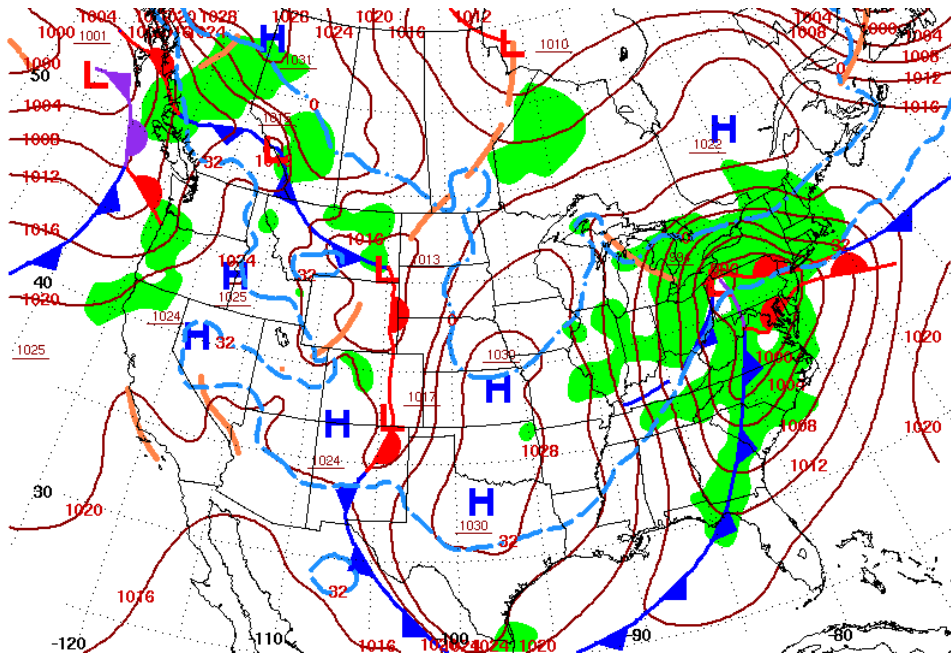
Lastly, it is also important to investigate the lowest level above the surface that the scan reached. Recall that the satellite radar scans do not reach all the way to the ground where the ASOS stations are located. Lowest Clutter Free Bin (LCFB) was lowest for HS with values rarely over 1000 m while it varied for MS and NS with values varying within the range stated earlier, 500-2500 m. Taking the difference between the LCFB and the lowest cloud deck (when reported) observed by ASOS from the surface reveals that for the majority of points, the lowest part of the scan was higher in altitude than the lowest cloud deck for all three scan modes, suggesting that any precipitation in the lowest cloud deck was not detected by DPR. The average difference for HS was 312.0 m, scanning closer than either MS or NS. The same average for MS was 742.3 m, more than double that of HS. NS was farthest from the lowest cloud levels with an average difference of 1093.8 m. Since NS has the widest scan, this

63

should be expected, especially since some of the largest values of LFCB are also found in NS.

*d)  16-17 February 2015 Winter Storm*

This event did not provide as many results as the previous case as there were only two swaths that passed over this system. Due to the types of precipitation that fell, it was important that this case be evaluated. The results are displayed in Table 20 and neither the High Sensitivity Scan (HS) nor Matched Scan (MS) performed significantly better than the other for this case. The only difference is that HS had more false liquid precipitation measurements whereas MS was more evenly distributed. With this case, all scans did have misses when detecting solid phase precipitation. The detection of these incidents is poor with detection rates ranging from 29% to 35%, with MS performing the best of the three.  In this case study, the scans did measure some liquid precipitation and all detected at least 75% of these occurrences. This is better than the previous case, but there was not as many observations in this storm. All scans have very few misses when nothing is observed.

Table 20: 16-17 February 2015 Case Study Hit/Miss. Hit/Miss chart for  16-17 February 2015 winter storm for HS, MS, and NS.

| | | DPR HS | | | |
|---|---|---|---|---|---|
| | | **Solid** | **Mixed** | **Liquid** | **Nothing** |
| **Surface Present Weather Observation** | **Solid** | 11 | 0 | 2 | 24 |
| | **Mixed** | 0 | 0 | 0 | 0 |
| | **Liquid** | 1 | 0 | 9 | 2 |
| | **Nothing** | 4 | 0 | 4 | 115 |

| Table 20 continued | | | | | |
|---|---|---|---|---|---|
| **DPR MS** | | | | | |
| | | **Solid** | **Mixed** | **Liquid** | **Nothing** |
| **Surface Present Weather Observation** | **Solid** | 14 | 0 | 3 | 23 |
| | **Mixed** | 0 | 0 | 0 | 0 |
| | **Liquid** | 1 | 0 | 10 | 1 |
| | **Nothing** | 3 | 0 | 4 | 125 |
| **DPR NS** | | | | | |
| | | **Solid** | **Mixed** | **Liquid** | **Nothing** |
| **Surface Present Weather Observation** | **Solid** | 22 | 0 | 4 | 51 |
| | **Mixed** | 0 | 0 | 0 | 0 |
| | **Liquid** | 3 | 0 | 15 | 2 |
| | **Nothing** | 3 | 0 | 6 | 262 |

Looking at Figure 26, this system had what appears to be a transition zone of liquid and solid precipitation. Unlike the previous case, DPR does better near this transition zone. The majority of misses appear to be in areas where DPR did not detect any precipitation. The group of six in Wisconsin stand out. The scan went over those stations within five minutes of the observed times. All six stations reported light snow. Despite detecting snow in NC, it failed to detect it in Wisconsin. This scan is an example of where results were included from the scan that may not necessarily be connected to the event focused on. For this particular

scan, including those points does count against the performance of DPR for the cases. However, it was beneficial to include those points with this case, because it exposes an event that DPR missed entirely.
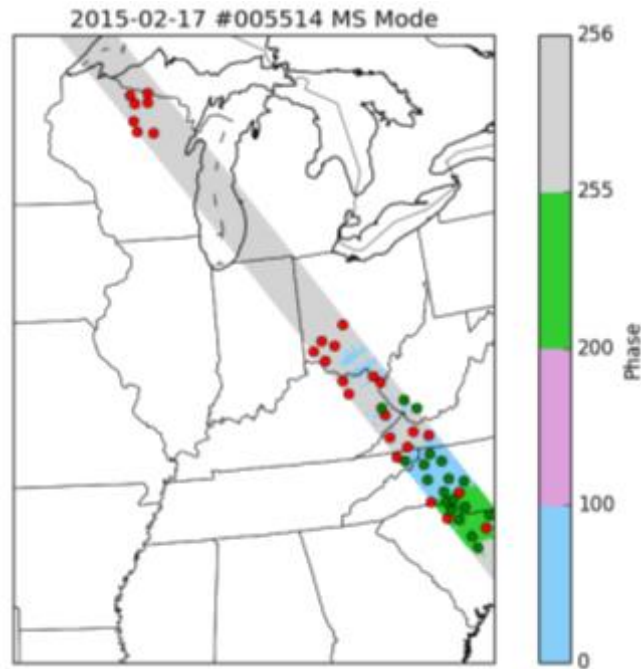


Figure 26. Scan #005514. Zoomed in view of phase of MS mode from scan #005514 on 17 February 2015 at 0153-0201 UTC with solid (blue), liquid (green), and no precipitation (gray) along the swath path. Green dots indicate locations where ground observations and DPR agreed. Red dots are where they did not. Dots are not shown for when both do not detect any precipitation.

Figure 27 shows one ground radar scan, KRLX, around the same time of this GPM scan. The majority of misses shown are when DPR did not detect precipitation. Many of those show locations where nothing was detected by DPR as well as the ground radar. With both unable to scan directly at the surface, it is hard to fault DPR for not detecting precipitation when ground radar shows the same thing. This ground radar scan also shows reflectivity values that are below the MDS of DPR, which a few of the misses fell within these areas. The KJKL radar (not shown) is located just to the southwest in Kentucky and shows many

misses where the phase of precipitation was missing from DPR's measurements but fall within areas of reflectivity values below DPR's MDS. Revisiting the misses in Wisconsin, ground radar was not available for this area. The Marquette radar in the Upper Peninsula was the closest radar within the vicinity of these stations. However, the scan did not extend far enough, and the beam height would have been much higher than DPR's lowest scan if it had detected precipitation. This is a good example of the additional lack of coverage in certain areas of CONUS, as this is one of many gaps in radar coverage. Due to unavailability of radar data in this area, it should be assumed that DPR simply missed the precipitation event in Wisconsin. Since it did miss, this snow event was probably below the minimum detectable signal of DPR.



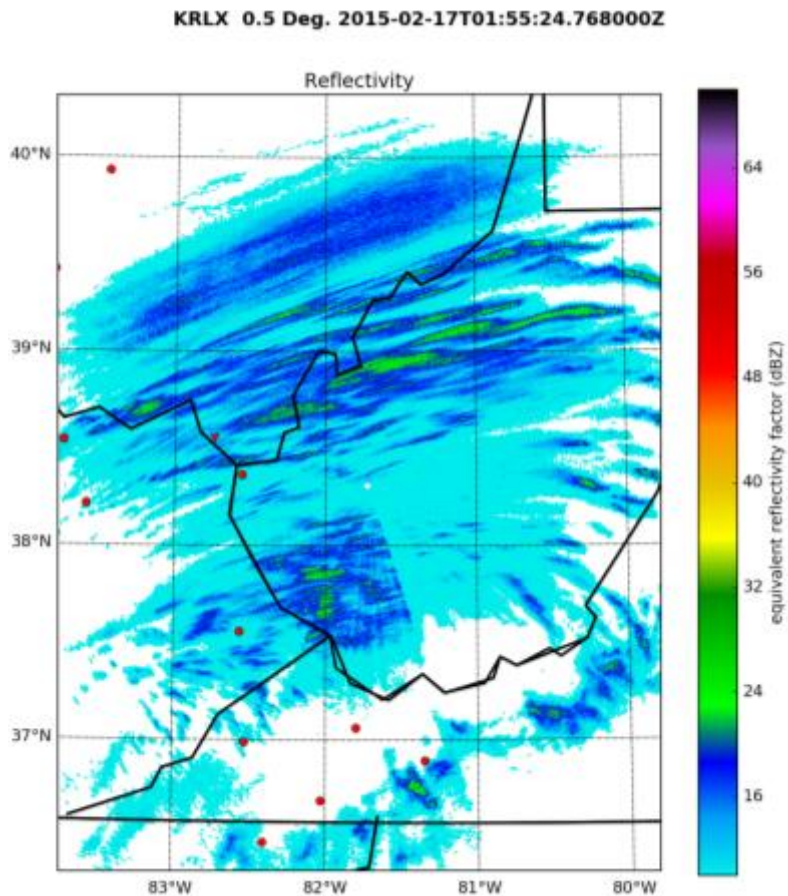KRLX 0.5 Deg. 2015-02-17T01:55:24.768000Z

Figure 27. KRLX Radar. The reflectivity of the lowest scan of KDIX Radar on 17 February 2015 at 0155 UTC. Misses, based on the Normal Scan mode from GPM scan #005514 are displayed circles, triangles, and squares. Circles are the misses when DPR did not detect precipitation but ground observations did. Triangles represent the misses when DPR did detect any precipitation but no Present Weather was reported by the ground observation.

Studying the incidents where DPR detected precipitation but no precipitation was reported at the ground reveals that there were also no precipitation amounts recorded at those stations. This is true for all scans and like the previous case, almost all of these stations fit the types of station that has the capability of reporting precipitation. Knowing this, it is highly likely that the ground stations are correct and other factors are responsible for the false detections. All three scans had one station, K4M9, where freezing rain (liquid) was observed but was measured as solid by DPR. For freezing rain, the precipitation remains a liquid until it contacts objects on the ground. In this case, the surface temperature was below freezing, suggesting that it may have fallen through a temperature inversion before reaching the ground and never refroze. The 00 UTC sounding from Little Rock (Figure 28) shows a strong, near-surface temperature inversion (warming with increasing altitude) where temperatures were much warmer than freezing. The surface temperature at 00 UTC was also warmer than freezing, but a few hours later when the observation was taken, the surface temperature had decreased. The forecast sounding, generated using Unidata's Integrated Data Viewer (IDV) from the Rapid Update Cycle (RUC) data archive available at http://mtarchive.geol.iastate.edu/, valid for the area around K4M9 and for the time of the observation, shows the below freezing temperatures at the surface. Using a forecast sounding closer to the location and timing of the observation should be more representative of the conditions in the atmosphere at that particular location than a sounding taken miles away.

The warmer air aloft and surface temperature changes shown in the Little Rock sounding would strongly support the claim that liquid precipitation, not ice, reached ground. The forecast sounding near K4M9 supports this as well. There is still a strong temperature inversion near the surface. The air temperature is also above freezing near the end of this inversion. With the sounding closer to the location and time of observation, the surface temperatures agree with those that were observed by the ground stations.

The other two incidents, stations KAVL and KINT located in NC, from the Normal Scan (NS) suggest a similar possibility as freezing rain was observed both stations with surface temperatures well below freezing, and DPR detected solid precipitation. The 06 UTC Greensboro Sounding on 17 February 2015 (not shown) reveals a strong temperature inversion with warmer-than-freezing temperatures above ground. The forecast sounding near KINT does show a strong temperature inversion but the air temperatures were just above freezing for a short period of time and was below freezing at the surface. The sounding near KAVL also shows an inversion but not nearly as strong. The air temperature does get above freezing during the inversion and was above freezing at the surface. Providing these soundings help support the DPR observations as solid precipitation would be observed at the surface without the strong temperature inversions near the surface. Showing the soundings in these cases does support DPR's measurements and helps explain why a different precipitation phase was detected at the surface.
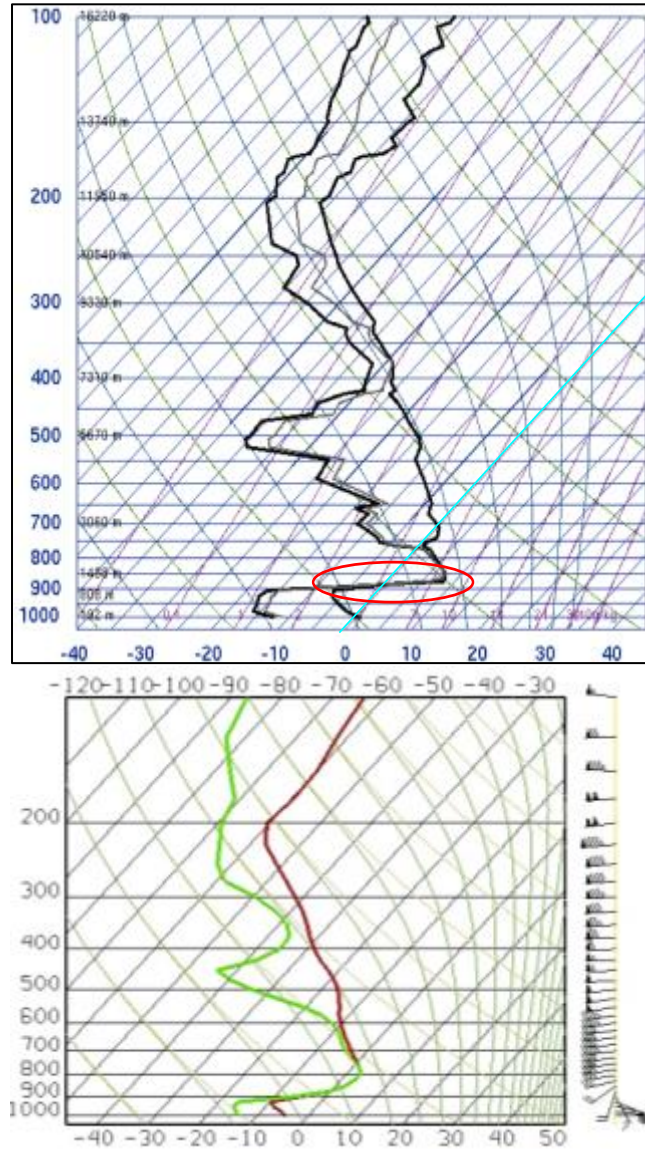
Figure 28: 16 February 2015 Soundings. (Top) 16 February 2015 0000 UTC sounding from Little Rock. The blue line indicates the freezing line. The red circle indicates a temperature inversion. The right black line indicates the temperature throughout the atmosphere (obtained from WYO 2017). (Bottom) A sounding generated from 0300 UTC RUC data and valid for 16 February 2015 at 0300 UTC. This forecast sounding represents the area the conditions over the K4M9 station around the time of the observation.

Studying the Lowest Clutter Free Bin (LCFB) for each scan shows similar results as the previous case. HS has the lowest average LCFB at 625 m and with NS having the highest average around 1368 m. The LCFB of HS was never over 1000 m. The differences between

70

the LCFB and lowest cloud deck reveal some interesting results. For HS, the average difference between the lowest cloud deck and scan height was negative meaning that it was scanning below the lowest cloud deck reported more often than scanning above. This same average difference for MS was slightly positive, which one would think there should have been some of these incidents detected by the scan. Revisiting those 6 misses in Wisconsin again, 5 of those stations reported cloud decks and the scan was below all them. Future work is needed to determine why DPR missed this particular snow event. As expected, NS has a positive average of around 468 m. As explained in the previous case, due to the wider scan, it will usually have higher LCFBs.

Since the LCFBs were calculated only for scans where DPR did not detect anything, the LCFB was calculated for K4M9, KAVL, and KINT separately. Recall for these observations, DPR had detected solid precipitation, but liquid precipitation was observed at the surface. The LCFB for the K4M9 location was 2204 m. When compared to the forecast sounding information and looking from the top down, the first height the air temperature was above freezing occurred at 2466 m when the temperature was 0.3°C. Since this is so close to 0°C, it is likely that most of the precipitation was ice that had not melted yet. The forecasted temperature did not fall below freezing again until around 1200 m. The sounding and observation K4M9 differed by about 1600 m for the cloud base. At KINT, the difference was small as both, the sounding and station, had the lowest cloud deck near the surface. The LCFBs for both locations were in freezing temperatures, meaning that DPR was correct in identifying solid precipitation. However, the LCFB at KINT was at a height that was still in the temperature inversion making it hard to determine what specifically would have been

71

observed at that height.

*e)  16-18 November 2015 Heavy Rain and Winter Storm*

This storm dropped snow over parts of the Rockies and Kansas and flooded many other areas along its path with heavy rainfall. Four scans were selected for this case study and one of the scans, see Figure 29, passed over an area of falling snow in Colorado. Despite detecting solid precipitation only a few times, it did correctly classify those occurrences. However, it failed to detect solid precipitation the majority of time with a poor detection rate of 18% for Normal Scan (NS), matching the 2-year results. Except for one miscue in the NS, DPR correctly classified the liquid precipitation. For instances where precipitation was observed at the surface but DPR did not detect any ($FN_s$, $FN_m$, or $FN_l$), the average Lowest Clutter Free Bottom (LCFB) values were similar to the previous two case studies. In this case study, the average difference between the LCFB and lowest cloud deck was positive for all three scan modes, meaning that the majority of scans were above the cloud deck. This is similar to the first case study. High Sensitivity Scan (HS) mode has the lowest average of about 279 m.

Figure 29 is the NS mode from scan #009767 on 17 November 2015. This scan passed over Colorado as the snow was falling. This figure shows clearly that DPR does not perform well not only over mountainous terrain, but also detecting snow over complex terrain. There were very few hits present in that scan. Figure 30 shows a variety of misses shown on the KFTG scan during GPM scan #009767. There are many misses along the outside that were not detected by DPR, but of those, there are instances where the ground radar shows either no

reflectivity or reflectivity values below DPR's MDS. Closer to the peak reflectivity values, there are a few misses when ground observations did not report Present Weather but DPR did detect precipitation. The KFTG scan shows the limitations of measurements with radars. Without being able to scan closer to the surface, radars may not detect precipitation observed at the surface.
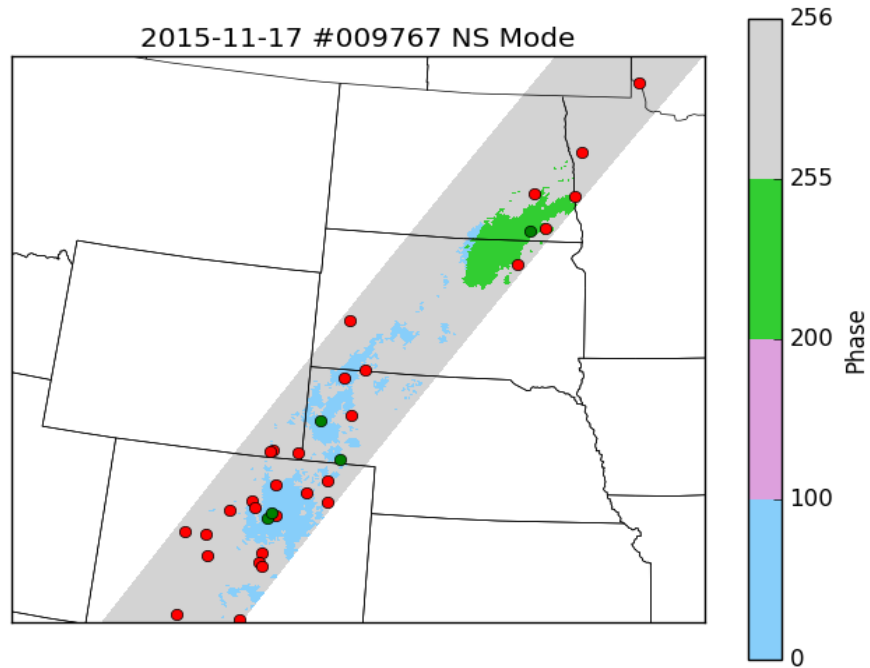


Figure 29. Scan #009767. The phase of NS mode from scan #009767 on 17 November 2015 at 1020-1029 UTC with solid (blue), liquid (green), and no precipitation (gray) along the swath path. Green dots indicate locations where ground observations and DPR agreed. Red dots are where they did not. Dots are not shown for when both do not detect any precipitation.
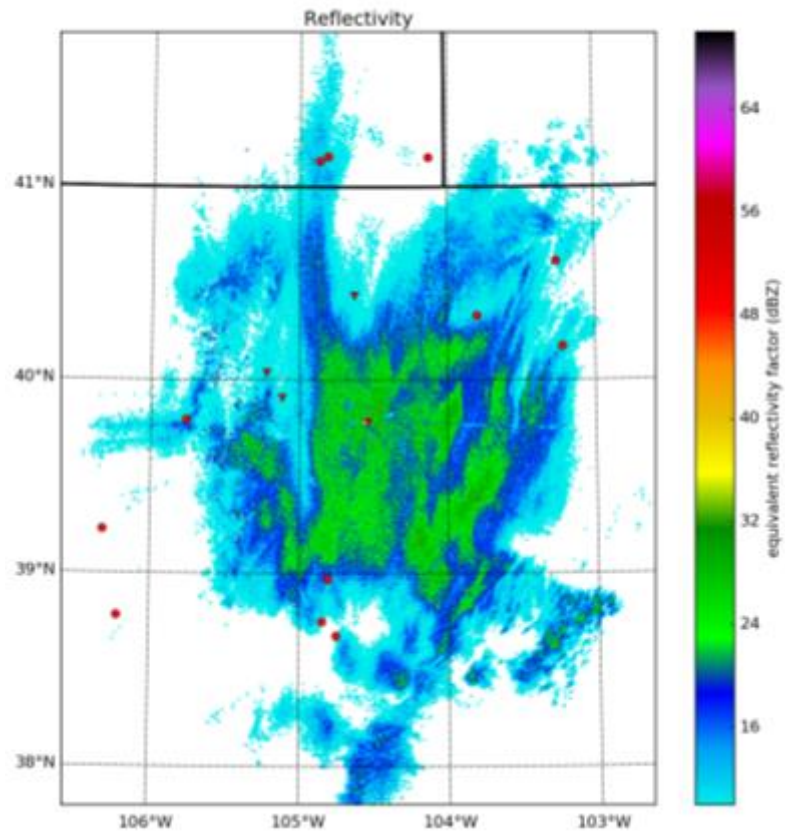
Figure 30. KFTG Radar. The reflectivity of the lowest scan of KFTG Radar on 17 November 2015 at 1035 UTC. Misses, based on the Normal Scan mode from GPM scan #009767 are displayed with circles, triangles, and squares. Circles are the misses when DPR did not detect precipitation but ground observations did. Triangles represent the misses when DPR did detect any precipitation bu t no Present Weather was reported by the ground observation.

Figure 31. Scan #009787. (Left) The phaseNearSurface of HS mode from scan #009787 on 18 November 2015 bottom at 1736-1744 UTC with solid (blue), liquid (green), and no precipitation (gray) along the swath path. Green dots indicate locations where ground observations and DPR agreed. Red dots are where they did not. Dots ar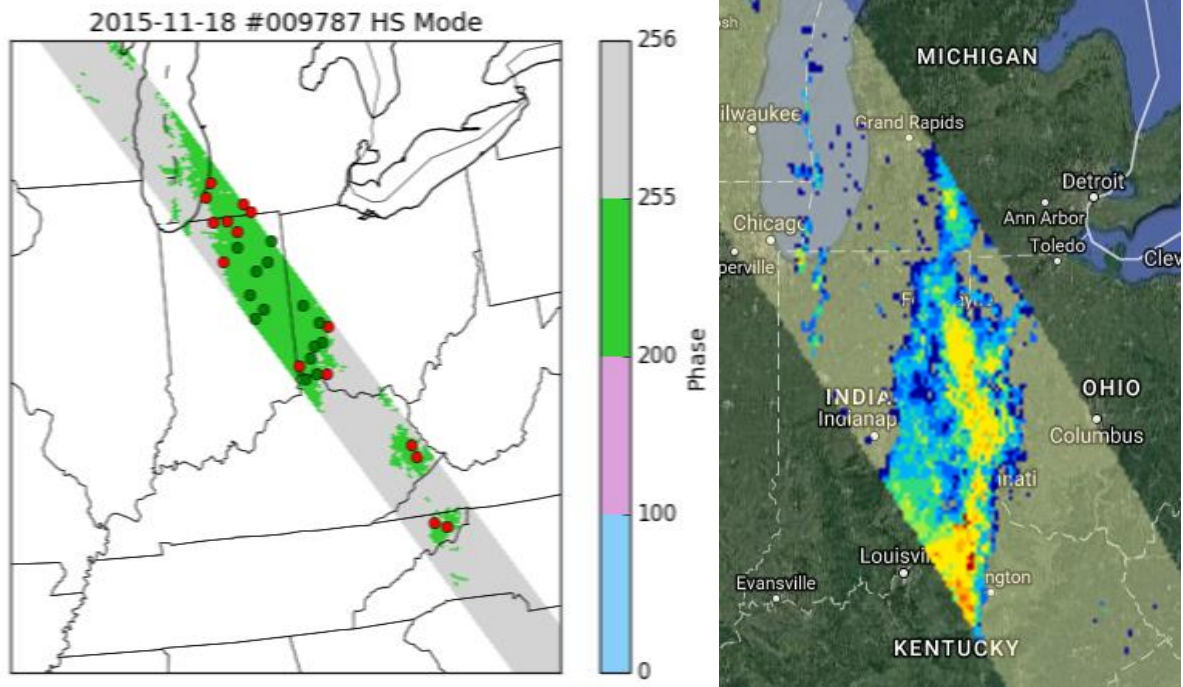e not shown for when both do not detect any precipitation. (Right) Precipitation rate from DPR scan #009787 is shown with blues indicating lighter precipitation (0.1-0.5 mm/hr) and reds indicating heavier precipitation (25-30 mm/hr) (JAXA 2017c).

Scan #009787 is displayed in Figure 31 to show that while DPR is not perfect, it does perform better when the precipitation is strictly liquid. The four misses in the southern portion of the scan are fairly close to the Appalachian Mountains which would suggest that DPR missed these due to complex terrain, but these four stations did not report a precipitation phase nor precipitation amounts. The time difference between the observation of three of these stations and the DPR observation pixel was around five minutes. For the other station, KTRI, the time difference was over 12 minutes. Ground radars in this area did not show precipitation over these stations, but there was precipitation to the west of their location around the time of GPM's overpass. The scan from ground radar KIWX, shown in

Figure 32, displays the misses observed in Northwestern Indiana. This is an interesting case because all the misses occurred when the ground observations did not report Present Weather or precipitation amounts. There is one miss in Ohio where this was also the case. This radar scan is also interesting because the misses fall in areas of no reflectivity or reflectivity values below DPR's MDS. When compared to the precipitation rates from DPR (Figure 31), this is similar to the scan from KWIX. Looking at the phase indicated by DPR in Figure 31, there seems to be an extension of the phase compared to the precipitation rates and ground radar scan. Considering this comparison, the phase of DPR resulted in misses due to the extended coverage of that variable.
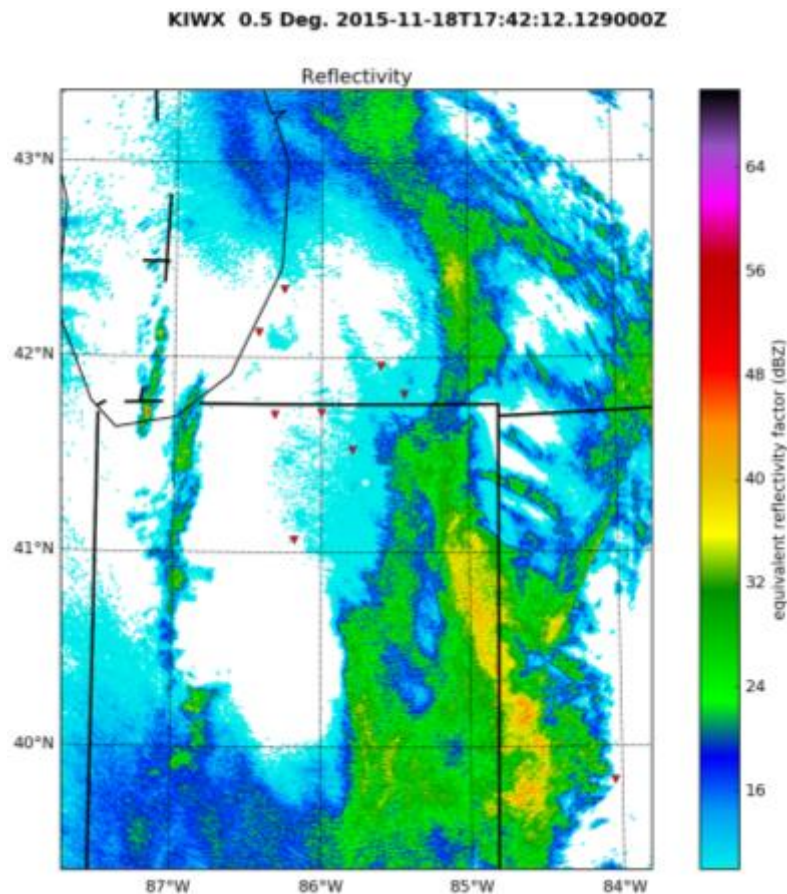


Figure 32. KIWX Radar. The reflectivity of the lowest scan of KIWX Radar on 18 November 2015 at 1742 UTC. Misses, based on the High Sensitivity Scan mode from GPM scan #009787 are displayed with circles, triangles, and squares. Triangles represent the

misses when DPR did detect any precipitation but no Present Weather was reported by the ground observation.

In this case study, there were many more instances where the satellite detected precipitation but nothing was reported at the surface. The values of hits and misses are displayed in Table 21. In HS mode, four out of the thirty-one (13%) incidents had present weather that was missing from the observation (sum of solid, mixed, and liquid under row "Nothing" in Table 21), but there was a precipitation amount reported. This was similarly true for, four out of twenty-six (15%) of the incidents for Matched Scan (MS) mode and five of forty-seven (11%) of the incidents for NS mode. In all the incidents where a precipitation amount was reported, DPR had classified these as liquid precipitation. In this case, there could be more hits if Present Weather had been available from the surface observations . For the rest of the possibilities, all but one of the stations are known to be equipped with precipitation instruments.

Table 21: 16-18 November Case Study Hit/Miss. Hit/Miss chart for 16-18 November 2015 Heavy Rain and Winter Storm for HS, MS, and HS.

| DPR HS | | | | | |
|---|---|---|---|---|---|
| | | **Solid** | **Mixed** | **Liquid** | **Nothing** |
| **Surface Present Weather Observation** | **Solid** | 4 | 0 | 0 | 8 |
| | **Mixed** | 0 | 0 | 0 | 0 |
| | **Liquid** | 0 | 0 | 27 | 18 |
| | **Nothing** | 4 | 0 | 27 | 195 |
| **DPR MS** | | | | | |
| | | **Solid** | **Mixed** | **Liquid** | **Nothing** |

| Surface Present Weather Observation | Table 21 continued | | | | |
|---|---|---|---|---|---|
| | **Solid** | 3 | 0 | 0 | 11 |
| | **Mixed** | 0 | 0 | 0 | 0 |
| | **Liquid** | 0 | 0 | 28 | 19 |
| | **Nothing** | 4 | 0 | 22 | 212 |

| DPR NS | | | | | |
|---|---|---|---|---|---|
| | | **Solid** | **Mixed** | **Liquid** | **Nothing** |
| **Surface Present Weather Observation** | **Solid** | 4 | 0 | 0 | 18 |
| | **Mixed** | 0 | 0 | 0 | 0 |
| | **Liquid** | 1 | 0 | 63 | 40 |
| | Table 21 continued | | | | |
| | **Nothing** | 5 | 0 | 42 | 423 |

CHAPTER V

SUMMARY AND CONCLUSIONS

This study focused on validating the phase measurements from the Global Precipitation Measurement Core Observatory (GPM-CO) satellite's Dual-frequency Precipitation Radar (DPR). It is important to study the performance of this instrument, as the satellite serves as calibration for other satellites in the GPM mission. GPM-CO is the second satellite to be equipped with a radar after the success of the Tropical Rainfall Measuring Mission (TRMM). The DPR onboard is the first spaceborne radar that can detect snow. Having the GPM-CO satellite and other satellites scanning the world provides continuous precipitation measurements over land and oceans. These measurements can help fill voids in surface observation and ground radar coverage.

Based upon previous work from Lott and Skofronick-Jackson 2017, this study took ground observations from CONUS between 15 March 2014 and 15 March 2016 and compared them with DPR phase measurements. The three scan modes, High Sensitivity Scan (HS), Matched Scan (MS), and Normal Scan (NS), from DPR were studied as each has different properties. The 2-year results show that DPR does not detect solid precipitation well with an overall detection rate of around 20% for mainly lower elevations and even worse in higher elevations. Despite this, when it does detect any precipitation, it does exceptionally well at correctly classifying the precipitation as solid with an overall hit rate of 97%. This matches the results found in Lott and Skofronick-Jackson (2017). Their smaller

study of investigating certain scans found that for light snow observations, DPR correctly classified solid precipitation 99% of the time, given that any precipitation was detected. This was 100% for moderate snow observations. Considering that the study herein included more observations and satellite scans than their study and the results were similar, this is promising for the future of not only GPM-CO but also future satellites that might be equipped with precipitation radars.

DPR performs better at detecting liquid phase precipitation. The detection rate is over 50% for lower elevated areas of CONUS. Studying areas mostly in the Rocky Mountains reveals that this detection rate is between 40 and 50%. DPR does not correctly classify liquid precipitation as well as it does solid precipitation, but in the eastern portion of CONUS in this study, the rate was around 94% for all scan types. However, this rate decreases to 85%, at best, for the west. MS performed better than HS, which was interesting as HS is designed to detect light rain which makes up for the majority of all rainfall. Even though these percentages are lower, DPR is successful in detecting liquid precipitation. While DPR does have a mixed phase category, this study did not find any results to support this measurement. The metrics calculated differ significantly from Speirs et al. (2017). The POD values for what is defined as complex terrain for both studies are similar only for the Speirs et al. (2017) cases for MeteoSwiss Radar and DPR scans above the freezing level. Their FAR values from their study are much lower than the findings this study. The skill scores also differ, but are positive in both studies. The differences between the values found in the studies can be explained by what was used as ground truth. When comparing a satellite radar and ground based radar, there are more data points in a given area than when ground stations are used.

Ground radars and satellite radars measure near the ground so there should be better agreement between them than when compared to ground stations. Measurements can differ between those taken at the surface compared to measurements taken at a height above the surface, as found this study.

Studying data with *qualityData* and *qualityFlag* does not change what was summarized in the previous paragraphs. Including these variables does improve the POD and HSS in most cases, but there are also cases where the FAR increases. Any decreases in detection and classification rates came from the western area. Overall, the performance improves with the addition of quality control. There were some files in Version 4 that were not included in the release Version 5, which might play a role in some of the changes seen between the two data sets. The Japanese Aerospace Exploration Agency may have made some undocumented changes to data in active files, but if changes were made, it is unclear what was changed. This could explain the some of the additional hits and misses. As far as comparing Version 5 data without quality variables against the Version 5 data with quality variables included, there will be no significant changes in the results. Doing this comparison for the first few months in this study shows that the quality variables eliminate results in the instances when DPR does not detect precipitation (Nothing column in Hit/Miss charts). Otherwise, there are no changes in the other hit and miss categories. Overall, it is important to include *qualityData* and *qualityFlag* variables so only good data is included in studies.

Individual case studies were investigated to help understand some of the misses from DPR. In two of the case studies, it was found that some of ground observation stations reported precipitation amounts but did not report present weather when DPR detected

precipitation. This would suggest that the problem is with the ASOS data and not the DPR. Thus, the detection rates found in the 2-year results might actually be better than originally found. For those that did not report present weather or precipitation amounts, most of the stations were equipped with precipitation instruments. In these cases, the stations are more likely to be correct and there was error in DPR. During the instances where DPR classified precipitation as solid but was reported as liquid at the surface, it is likely that the DPR was sensing the ice aloft which melted before reaching the surface. Forecast soundings closer to these ground observations does support the observed soundings, especially the sounding near K4M9 as the forecasted and observed seemed to be in the best agreement. Studying the misses when DPR did not detect precipitation reveals that the higher scan height for MS and NS could be a factor for these misses, but does not show the same support for HS.

Including ground radar scans in the case studies showed many instances where DPR did not detect precipitation but might be explained by the lack of reflectivity from the ground radar and reflectivity values below DPR's minimum detectable signal (MDS). With the results from these ground radar scans, it is difficult to fault DPR for not detecting precipitation. While much rarer, there were some instances where ground observations did not report Present Weather, but as explained earlier, this might due to not having the sensors to be able to report this. While not investigated, radar composites, maximum reflectivity values at any level, could show more support for DPR measurements as well. In the 16-18 November case study, it was determined that the *phaseNearSurface* of DPR was reported even though DPR itself did not have measured precipitation rates at the same location. This was verified using a ground radar scan. The reason for this issue was not studied, but using

two variables from DPR could justify its measurements.

While not studied in depth, possibly greater time differences between the DPR scan and surface observation could explain at least some of these misses. Time differences did vary for misses anywhere from a couple of seconds to almost the full 30 minutes. The timing of the event itself may matter more than the time differences between the ground observations and the GPM overpass. Taking two observations from the same location with the closest times to DPR measurements could reveal that two types of weather conditions were observed between the time of the two observations. This might explain some of the differences between DPR and ground observations. Another possible error that was not studied in depth could be in the ground station observations. While the exact errors are unknown, there could be error in the identification of precipitation particles, especially in cases where surface temperature is around 0°C.

The findings in this study provide evidence that DPR is detecting solid precipitation. If DPR detects precipitation, then it is performing well at distinguishing between liquid and solid phases. Even though factors were explored to justify the incidents where ground observations and DPR do not agree, issues with DPR are also a possibility. With the success of the GPM mission, scientists will gain a better understanding of the water cycle, be able to implement the data in numerical weather prediction models, and will be able monitor fresh water resources more closely. Just like the TRMM satellite, the GPM-CO satellite will be a learning tool for any future satellites equipped with precipitation detecting radars.

CHAPTER VI

FUTURE WORK

This study could be expanded to use three years of data or even more to validate phase measurements. Additional years could provide insight on any changes in performance. One known issue found in this study was the instances when AWOS/ASOS stations did not report Present Weather but recorded a precipitation amount when DPR detected precipitation. A similar issue with DPR is that phase is reported even though there was not a precipitation amount measured. This study could be performed again, but use two variables from each to justify their measurements. Doing this could improve the results of DPR's precipitation phase classification especially the instances when nothing was detected by the ground station. Incorporating NSSL's MRMS would increase coverage and could result in more and improved results.

APPENDIX

ACRONYMS

| | |
|---|---|
| AGL | Above Ground Level |
| ASOS | Automated Surface Observing System |
| AWOS | Automated Weather Observing Station |
| BB | bright band |
| C3VP | Canadian CloudSAT/Calipso Validation Program |
| CCC | Colorado Climate Center |
| CDF | cumulative density function |
| CNES | Centre National D'Etudies Spatiales |
| CoCoRaHS | Community Collaborative Rain, Hail, and Snow Network |
| CONUS | Contiguous United Station |
| CSF | Classification |
| DEM | digital elevation model |
| $DFR_m$ | measured dual frequency ratio |
| DMSP | Defense Meteorological Satellite Program |
| DOC | Department of Commerce |
| DPR | Dual-frequency Precipitation Radar |
| DSD | Raindrop Size Distribution |
| FAA | Federal Aviation Administration |

| | |
|---|---|
| FAR | false alarm rate |
| FMH1 | Federal Meteorological Handbook 1 |
| FN | false negative |
| FP | false positive |
| GCOM-W1 | Global Change Observation Mission-Water 1 |
| GCPEx | GPM Cold-season Precipitation Experiment |
| GPCC | Global Precipitation Climatology Centre |
| GPCP | Global Precipitation Climatology Project |
| GPM | Global Precipitation Measurement |
| GPM-CO | Global Precipitation Measurement Core Observatory |
| GTS | Global Telecommunication System |
| HS | High Sensitivity Scan |
| HSS | Heidke Skill Score |
| IEM | Iowa Environment Mesonet |
| IFloodS | Iowa Flood Studies |
| IPHEx | Integrated Precipitation and Hydrology Experiment |
| ISRO | Indian Space Research Organization |
| JAXA | Japan Aerospace Exploratory Agency |
| JPSS | Joint Polar Satellite System |
| KaPR | Ka-band Precipitation Radar |
| KuPR | Ku-band Precipitation Radar |
| LCFB | Lowest Clutter Free Bin |

| LIS | Land Information System |
| LPVEx | Light Precipitation Evaluation Experiment |
| MC3E | Mid-Continent Convective Clouds Experiment |
| MDS | minimum detectable signal |
| mPING | Meteorological Phenomena Identification Near the Ground |
| MRMS | Multi-Radar/Multi-Sensor |
| MS | Matched Scan |
| NASA | National Aeronautics and Space Administration |
| NEXRAD | Next-Generation Radar |
| NICAM | Nonhydrostatic Icosahedral Atmospheric Model |
| NICT | National Institute of Information and Communications Technology of Japan |
| NIST | National Institute of Standards and Technology |
| NOAA | National Oceanic and Atmospheric Administration |
| NOHRSC | National Operational Hydrologic Remote Sensing Center |
| NPOESS | National Polar-Orbiting Operational Environment Satellite System |
| NPOL | NASA's S-band dual-polarized radar |
| NPP | NPOESS Preparatory Project |
| NS | Normal Scan |
| NSSL | National Severe Storms Laboratory |
| OLYMPEX | Olympic Mountains Experiment |
| POD | probability of detection |
| POES | Polar-Orbiting Operational Environment Satellite |

PPS         Precipitation Processing System

PR          precipitation radar

PREP        Preparation

QC          Quality Control

SLV         Solver

SMAP        Soil Moisture Active Passive

THOR        Tool for High-resolution Observation Review

TN          true negative

TP          true positive

TRMM        Tropical Rainfall Measuring Mission

UCAR        University Corporation for Atmospheric Research

UND         University of North Dakota

UTC         Coordinated Universal Time

WMO         World Meteorological Organization

WPC         Weather Prediction Center

WOW         Weather Observations Website

REFERENCES

Alder, R., S. Braun, E. Stoker, and J. Marius, 2007: Tropical Rainfall Measuring Mission
TRMM Senior Review Proposal. 50 pp.

All Weather Inc., 2014: FAA Certified AWOS. Accessed 21 May 2017. [Available online at
http://www.allweatherinc.com/domestic-automated-weather-observation
system/#tabs=581.]

Barros, A. P. and Coauthors, 2014: NASA GPM-Ground Validation Integrated Precipitation
and Hydrology Experiment 2014: Science Plan. 64 pp. [Available online at
https://dukespace.lib.duke.edu/dspace/bitstream/handle/10161/8991/IPHEX-
v5.pdf?sequence=1.]

Braun, C., 2011:  Tropical Rainfall Measuring Mission Senior Review Proposal 2011. 58 pp.
[Available online at
https://pmm.nasa.gov/sites/default/files/document_files/TRMMSenRevProp_v1.2.pdf.]

Campbell Scientific, 2014: Changes to Visibility and Present-Weather Sensors. Accessed on
25 July 2017. [Available online at https://www.campbellsci.com/news-cs125-cs120a.]

Chandrasekar, V., M. Le, and S. Biswas, 2016: Snowfall on the Ground Identifier and
Validation for DPR. *8th IPWG and 5th IWSSM Joint Workshop*. Bologna, Italy.
International Precipitation Working Group, 5.5. [Available online at
http://www.isac.cnr.it/~ipwg/meetings/bologna-2016/Bologna2016_Orals/5
-5_Chandra.pdf.]

Colorado Climate Center (CCC), 2016: CoCoRaHS About Us. Accessed 3 February 2017.

[Available online at http://www.cocorahs.org/Content.aspx?page=aboutus.]

_____, 2017: Maps: Weather Stations. Accessed 22 June 2017. [Available online at

http://www.cocorahs.org/Maps/ViewMap.aspx?type=stations.]

Department of Commerce (DOC), 2017: Daily Weather Maps. Weather Prediction Center.

Accessed 22 June 2017. [Available online at

http://www.wpc.ncep.noaa.gov/dailywxmap/.]

EUMETSAT, 2017: METOP. Accessed 11 June 2017. [Available online at

http://www.eumetsat.int/website/home/Satellites/CurrentSatellites/Metop/index.html.]

FAA, 2016: Surface Weather Observation Stations ASOS/AWOS. Accessed 21 May 2017.

[Available online at https://www.faa.gov/air_traffic/weather/asos/].

Galimbertie, K., 2014: RECAP: California Storm Leaves a Trail of Destruction.

AccuWeather. Accessed 18 May 2017. [Available online at

http://www.accuweather.com/en/weather-news/california-bay-area-storm-

floo/38828635.]

Gruss, M., 2016: Air Force says DMSP-19 Weather Satellite is "About Dead". Space News.

Accessed 12 June 2017. [Available online at http://spacenews.com/air-force-says-dmsp-

19- weather-satellite-is-about-dead/.]

Hamada, A. and Y. Takayabu, 2016: Improvements in Detection of Light Precipitation with

the Global Precipitation Measurement Dual-Frequency Precipitation Radar (DPR). J.

Atmos. Oceanic Technol., 33, 653–667, doi: 10.1175/JTECH-D-15-0097.1.

Hanson, H. and E. Gray, 2012: Global Precipitation Measurement Core Observatory

Brochure. 17 pp.

Hou, A. Y., 2000: Lesson from TRMM and Plans for GPM. *ECMWF/EuroTRMM Workshop*
*on the Assimilation of Clouds and Precipitation*, Shinfield, Reading, ECMWF.
[Available online  at https://www.ecmwf.int/sites/default/files/elibrary/2000/10036-
lessons-trmm-and-plans-gpm.pdf.]

_____, and Coauthors, 2014: The Global Measurement System Mission. *Bull. Amer.*
*Meteor.     Soc.*, 95, 701-722.

Houze, R.A. and Coauthors, 0: The Olympic Mountains Experiment (OLYMPEX). *Bull.*
*Amer.  Meteor. Soc.*, 0, doi: 10.1175/BAMS-D-16-0182.1.

Iguchi, T., S. Seto, R. Meneghini, N. Yoshida, J. Awaka, M. Le, V. Chandrasekar, and T.
Kubota, 2016: GPM/DPR Level-2 Algorithm Theoretical Basis Document Revised
March  2016 version, 68 pp.

_____, S. Seto, R. Meneghini, N. Yoshida, J. Awaka, M. Le, V. Chandrasekar, and T.
Kubota, 2016: GPM/DPR Level-2 Algorithm Theoretical Basis Document Revised April
2017 version, 79 pp.

JAXA, 2017a: Overview of GPM Products. 2.1. 80 pp. [Available online at
http://www.eorc.jaxa.jp/GPM/doc/product/format/en/01.%20Overview%20of%20GPM%
20Products_E.pdf.]

_____, 2017b: Release Notes for the DPR V5 Level 2 Products. Accessed on 20 July 2017.
[Available online at
https://pps.gsfc.nasa.gov/Documents/V05ReleaseNotes/Caveats_DPRL2_productV05.pdf
.]

_____, 2017c: GPM Quick Look. Accessed on 25 July 2017. [Available online at

　http://sharaku.eorc.jaxa.jp/trmm/QL/.]

Kidd, C., A. Becker, G. Huffman, C. Muller, P. Joe, G. Skofronick-Jackson, and D.

　Kirschbaum, 2017: So, how much of the Earth's surface is covered by rain gauges?. *Bull.*

　*Amer. Meteor. Soc.,* **98**, doi: 10.1175/BAMS-D-14-00283.1.

Krekeler, J., 2015: Southwest to Northeast Winter Storm Event Review. Accessed 16 May

　2017.

　[Available online at

　http://www.wpc.ncep.noaa.gov/winter_storm_summaries/event_reviews/2015/Southwest

　_Northeast_WinterStorm_Jan2015.pdf.]

_____, 2016: Central U.S. Winter Storm Event Review. Accessed 27 May 2017. [Available

　online at

　http://www.wpc.ncep.noaa.gov/winter_storm_summaries/event_reviews/2015/Central_U

　S_ WinterStorm_Nov2015.pdf.]

Kotsuki, S., K. Terasaki, and T. Miyoshi, 2014: GPM/DPR Precipitation Compared with a

　3.5-km-Resolution NICAM Simulation. *Scientific Online Letters of the Atmosphere*. **10**,

　doi:10.2151/sola.2014-043.

Le, M., V. Chandrasekar, and S. Biswas, 2016. Evaluation and Validation of GPM Dual-

　Frequency Classification Module After Launch. J. Atmos. Oceanic Technol., 33, 2699-

　2716,　doi:10.1175/JTECH-D-15-0253.1.

Liao, L. and R. Meneghini, 2009: Validation of TRMM Precipitation Radar through

　Comparison of Its Multiyear Measurements with Ground-Based Radar. *J. Appl. Meteor.*

*Climatol.,* **48**, 804–817, doi.org/10.1175/2008JAMC1974.1

Lott, B. T. and G. Skofronick-Jackson, 2017: Validation of Satellite Snowfall Measurements

    in   CONUS. *Observation Symposium: Progress, Problems, and Prospects*, Seattle, WA,

    Amer. Meteor. Soc., 1021. [Available online at

https://ams.confex.com/ams/97Annual/webprogram/Paper308992.html.]

NASA, 2012: JAXA Launches GCOM-W1 Satellite. Accessed 11 June 2017. [Available

    online at https://www.nasa.gov/mission_pages/GPM/news/jaxa_gcomw1_launch.html.]

_____, 2014: Precipitation Processing System Global Precipitation Measurement: File

Specification for GPM Products, 1311 pp. [Available online at

https://storm.pps.eosdis.nasa.gov/storm/filespec.GPM.V1.pdf.]

_____, 2015: STORM. Accessed 10 January 2017. [Available online at

https://storm.pps.eosdis.nasa.gov/storm/.]

_____, 2017a: Precipitation Measurement Missions: Constellation Partners. Accessed 10

    June 2017. [Available online at https://pmm.nasa.gov/GPM/constellation-partners.]

_____, 2017b: Precipitation Measurement Missions: Ground Validation. Accessed 27 May

    2017.

[Available online at https://pmm.nasa.gov/science/ground-validation.]

_____, 2017c: NASA Space Science Data Coordinated Archive. Accessed 11 June 2017.

[Available online at https://nssdc.gsfc.nasa.gov/nmc/SpacecraftQuery.jsp.]

_____, 2017d: Satellite Safety. Accessed 11 July 2017. [Available online at

https://satellitesafety.gsfc.nasa.gov/gpm.html.]

_____, 2017e: Algorithm Format Changes from Version 4 to Version 5. Accessed 20 July

2017. [Available online at

https://pps.gsfc.nasa.gov/Documents/V05ReleaseNotes/GPM%20Algorithm%20Format

%20Changes%20From%20V4%20to%20V5%20in%20Algorithm%20Order_May%2020

17.pdf.]

National Institute of Standards and Technology (NIST), 2003: Engineering Statistics

Handbook. Accessed 17 February 2017. [Available online at

http://www.itl.nist.gov/div898/handbook/eda/section3/eda362.htm.]

NOAA, 2016: NEXRAD and TDWR Radar Locations. Accessed 13 February 2017.

[Available online at https://www.roc.noaa.gov/wsr88d/maps.aspx.]

NOAA, 2017a: Joint Polar Satellite System: Mission and Instruments. Accessed 11 June

2017.  [Available online at http://www.jpss.noaa.gov/mission_and_instruments.html.]

NOAA, 2017b,: NEXRAD Technical Information. NOAA. Accessed 20 July 2017.

[Available online at

https://www.roc.noaa.gov/WSR88D/Engineering/NEXRADTechInfo.aspx.]

NOHRSC, 2017: Interactive Snow Information. NOAA. Accessed 22 June 2017.

[Available online at https://www.nohrsc.noaa.gov/interactive/html/map.html.]

NSSL, 2017: Research Tools: Multi-function Phased Array Radar. NSSL. Accessed 14 July

2017. [Available online at http://www.nssl.noaa.gov/tools/radar/mpar/.]

NWS, 2015: National Weather Service Reference Guide *Chapter 8. Equipment*. National

Weather Service. pp 123-133.

Pierce, H, 2017: TRMM Tropical Rainfall Measurement Mission. Accessed 12 February

2017. [Available online at https://trmm.gsfc.nasa.gov/.]

Read, W., 2014: The Classic Windstorm of December 11, 2014. Accessed 18 May 2017.

   [Available online at http://www.climate.washington.edu/stormking/December2014.html.]

Rémy, R. and Coauthors, 2015: The Megha-Tropiques Mission: A Review After Three Years

   in  Orbit. Frontiers in Earth Science, 3, doi: 10.3389/feart.2015.00017. [Available online

   at http://journal.frontiersin.org/article/10.3389/.]

Santorelli, A., 2015: Southern Plains to Mid-Atlantic Winter Storm Event Review. Accessed

   16 May 2017. [Available online at

   http://www.wpc.ncep.noaa.gov/winter_storm_summaries/event_reviews/2015/SouthernPl

   ains_MidAtlantic_WinterStorm_Feb2015.pdf.]

Schwaller, M.R. and K.R. Morris, 2011: A Ground Validation Network for the Global

   Precipitation Measurement Mission. J. Atmos. Oceanic Technol., 28, 301–319, doi:

   10.1175/2010JTECHA1403.1.

Seto, S., T. Iguchi, R. Meneghini, J. Awaka, T. Kubota, and N. Yoshida, 2011: Current

   Status of the Dual-frequency Precipitation Radar (DPR) Level-2 Standard Algorithm

   Development. *35th Conference on Radar Meteorology*, Pittsburgh, PA, Amer. Meteor.

   Soc., 11B.2. [Available online at

   https://ams.confex.com/ams/35Radar/webprogram/Paper191944.html.]

Skofronick-Jackson, G., 2011: Precipitation Measurement Systems: Global Precipitation

   Measurement. NASA. Accessed 26 July 2016. [Available online at

   https://pmm.nasa.gov/GPM.]

_____, and Coauthors, 2015: Global Precipitation Measurement Cold Season  Precipitation

   Experiment (GCPEX): For Measurement's Sake, Let it Snow. *Bull. Amer. Meteor. Soc.,*

**96**, 1719-1741. doi:10.1175/BAMS-D-13-00262.1

_____, and Coauthors, 2016a: The Global Precipitation Measurement (GPM) Mission for Science and *Society. Bull. Amer. Meteor. Soc.* doi:10.1175/BAMS-D-15-00306.1, in press.

_____, S. J. Munchak, and S. Ringerud, 2016b: Performance of the Falling Snow Retrieval Algorithms for the Global Precipitation Measurement (GPM) Mission. *Proc. IEEE Int. Conf. on Geoscience and Remote Sensing Symp. 2016,* Beijing, China, Institute of Electrical and Electronics Engineers, 2139-2141, doi:10.1109/IGARSS.2016.7729552.

Speirs, P., M. Gabella, and A. Berne, 2017: A Comparison between the GPM Dual-Frequency Precipitation Radar and Ground-Based Radar Precipitation Rate Estimates in the Swiss Alps and Plateau. J. Hydrometeor., 18, 1247–1269, doi: 10.1175/JHM-D-16-0085.1.

UCAR, 2006: Clouds, Precipitation, & Water Vapor COMET Module Print Version. [Available online at http://www.meted.ucar.edu/npoess/microwave_topics/clouds_precip_water_vapor/print.htm.]

U.S. DOC/NOAA, 2005: Federal Meteorological Handbook 1: Surface Weather Observations and Reports. 104 pp. [Available online at http://www.ofcm.gov/publications/fmh/FMH1/FMH1.pdf.]

Wawrzyniak, T., C. J. Melick, P. T. Marsh, and J. Picca, 2017: Evaluation of Precipitation Type from Observational Datasets to Improve Monitoring of Hazardous Winter Weather at the Storm Prediction Center. *33rd Conference on Environmental Information*

*Processing Technologies*, Seattle, WA, Amer. Meteor. Soc., J9.4. [Available online at

https://ams.confex.com/ams/97Annual/webprogram/Paper315522.html.]

Wolff, C., 2017: Phased Array Antenna. Accessed 14 July 2017. [Available online at

http://www.radartutorial.eu/06.antennas/Phased%20Array%20Antenna.en.html.]

University of Wyoming (UWY), 2017: Department of Atmospheric Science Soundings.

Accessed 15 July 2017. [Available online at

http://weather.uwyo.edu/upperair/sounding.html.]

WPC, 2014: Powerful West Coast Storm: Storm Summaries 1-7. NWS. Accessed 18 May

2017.

[Available online at

http://www.wpc.ncep.noaa.gov/winter_storm_summaries/2014/storm29/storm29_archive

.shtml.]

＿＿＿, 2015: Central to Eastern U.S. Heavy Rain and Winter Storm: Storm Summaries 1-9.

NWS. Accessed 27 May 2017. [Available online at

http://www.wpc.ncep.noaa.gov/winter_storm_summaries/2015/storm18/storm18_archive

.shtml.]

＿＿＿, 2017: 2017 Storm Summaries. NWS. Accessed 18 May 2017. [Available online at

http://www.wpc.ncep.noaa.gov/winter_storm_summaries/winter_storm_summaries.shtml

.]